Brain Structure and Function (2024) 229:1533–1559
https://doi.org/10.1007/s00429-024-02807-2

ORIGINAL ARTICLE

Age-related differences in resting-state, task-related, and structural brain connectivity: graph theoretical analyses and visual search performance

David J. Madden[1,2,3] · **Jenna L. Merenstein**[1] · **Hollie A. Mullin**[1,5] · **Shivangi Jain**[1,6] · **Marc D. Rudolph**[4,7] · **Jessica R. Cohen**[4]

Received: 29 December 2023 / Accepted: 13 May 2024 / Published online: 10 June 2024

Abstract

Previous magnetic resonance imaging (MRI) research suggests that aging is associated with a decrease in the functional interconnections within and between groups of locally organized brain regions (modules). Further, this age-related decrease in the segregation of modules appears to be more pronounced for a task, relative to a resting state, reflecting the integration of functional modules and attentional allocation necessary to support task performance. Here, using graph-theoretical analyses, we investigated age-related differences in a whole-brain measure of module connectivity, *system segregation*, for 68 healthy, community-dwelling individuals 18–78 years of age. We obtained resting-state, task-related (visual search), and structural (diffusion-weighted) MRI data. Using a parcellation of modules derived from the participants' resting-state functional MRI data, we demonstrated that the decrease in system segregation from rest to task (i.e., reconfiguration) increased with age, suggesting an age-related increase in the integration of modules required by the attentional demands of visual search. Structural system segregation increased with age, reflecting weaker connectivity both within and between modules. Functional and structural system segregation had qualitatively different influences on age-related decline in visual search performance. Functional system segregation (and reconfiguration) influenced age-related decline in the rate of visual evidence accumulation (drift rate), whereas structural system segregation contributed to age-related slowing of encoding and response processes (nondecision time). The age-related differences in the functional system segregation measures, however, were relatively independent of those associated with structural connectivity.

Keywords Aging · Cognition · Visual perception · Attention · Brain networks · MRI

✉ David J. Madden
david.madden@duke.edu

1 Brain Imaging and Analysis Center, Duke University Medical Center, Box 3918, Durham, NC 27710, USA

2 Department of Psychiatry and Behavioral Sciences, Duke University Medical Center, Durham, NC 27710, USA

3 Center for Cognitive Neuroscience, Duke University, Durham, NC 27708, USA

4 Department of Psychology and Neuroscience, University of North Carolina at Chapel Hill, Chapel Hill, NC 27514, USA

5 Present Address: Department of Psychology, Pennsylvania State University, University Park, PA 16802, USA

6 Present Address: AdventHealth Research Institute, Neuroscience Institute, Orlando, FL 32804, USA

7 Present Address: Department of Internal Medicine, Wake Forest University School of Medicine, Winston-Salem, NC 27101, USA

Introduction

Recent developments in graph theoretical analyses (Bullmore and Sporns 2009; Rubinov and Sporns 2010; Sporns 2011; Sporns and Betzel 2016) have led to a characterization of the human brain as a network of regions (nodes) with structural or functional connections between nodes (edges). This network may be partitioned into distinct sets of interconnected nodes (modules). To date, findings derived primarily from younger adults suggest that the brain exhibits characteristically small-world properties, with strong local connectivity (interconnectivity within modules), and fewer long-range connections between modules. These small-world properties, especially the presence of modules, are hypothesized to allow the brain to adapt efficiently to changing cognitive demands in the environment (Crossley et al. 2013; Mišić and Sporns 2016).

Functional brain networks

Graph theoretical analyses of functional brain connectivity have been developed predominantly from resting-state functional magnetic resonance imaging (fMRI), which measures the correlations among the fMRI time series of selected nodes, in the absence of an ongoing cognitive or behavioral task (Achard and Bullmore 2007; Power et al. 2011; Yeo et al. 2011). These types of analyses, however, can also be used to characterize functional connectivity during task performance (Cisler et al. 2014; Mumford et al. 2012; Rissman et al. 2004). Studies implementing graph theoretical analyses suggest a close correspondence in the architectures of resting-state and task-related functional connectivity. Functional connectivity during tasks appears to reflect the influence of a limited number of modules, identifiable from a resting state, which are then differentially engaged by specific task demands (Bolt et al. 2017; Cole et al. 2014; Krienen et al. 2014).

Direct comparison of resting-state and task-related functional connectivity suggests that, in the context of an overall similarity in small-world architecture, some features of the whole-brain network reconfigure during a cognitive task, relative to the resting state. Whereas modules are segregated during rest, and during simple tasks (e.g., motor execution), different modules become more integrated during the performance of more complex cognitive tasks, presumably representing the coordination of multiple components of cognition (Braun et al. 2015; Cohen and D'Esposito 2016; Cohen et al. 2014; Wen et al. 2015; Shine et al. 2016; Elton and Gao 2015). In the case of visuospatial attention, for example, functional connectivity between visual and dorsal frontoparietal modules increases during task performance, relative to rest (Spadone et al. 2015).

Structural brain networks

Graph theoretical analyses can also characterize structural connectivity networks, which are typically estimated from streamlines identified in diffusion-weighted imaging (DWI), where the number of streamlines between nodes reflects connectivity strength (Fan et al. 2016; Hagmann et al. 2007). These anatomical connections among brain nodes also exhibit small-world properties, and the strength of these structural connections appears to shape the organization of functional connectivity (Barttfeld et al. 2015; Gong et al. 2009; Hagmann et al. 2008). However, functional and structural networks differ qualitatively, in that functional networks are more densely connected, comprising both direct and indirect connections, as well as negative correlations between nodes (Zuo et al. 2017; Civier et al. 2019; van Wijk et al. 2010). Thus, functional modules do not necessarily correspond node-to-node to the underlying structural network, and a particular structural network configuration may support different, non-overlapping functional configurations (Mišić et al. 2016).

Aging and network reconfiguration

Here, we investigated age-related differences in the reconfiguration of functional connectivity, from resting to task states, as well as the relation of reconfiguration to structural connectivity and cognitive performance (visual search). The term reconfiguration can refer to either the change in modular organization between rest and task (Gallen et al. 2016; Hearne et al. 2017), or to the change in connectivity strength between rest and task for a pre-defined set of modules (Cohen et al. 2014). We use the term in the latter sense, deriving the set of modules, or network partition, empirically from the resting-state data for the whole sample. Whereas graph theory provides a variety of measures relevant for understanding reconfiguration, we focus here on *system segregation*, which represents the degree to which modules within a whole-brain network are distinct from each other. Conceptually, system segregation can be viewed as the relative strength of within-module connectivity as compared to between-module connectivity, so that an increasing predominance of within-module connectivity is expressed as increased system segregation. A prominent theme in graph theoretical analyses of aging is that age-related decline occurs in system segregation for resting-state functional connectivity (Chan et al. 2014; Deery et al. 2023; Goh 2011; Madden et al. 2020a; Malagurski et al. 2020; Ng et al. 2016; Pedersen et al. 2021; Wig 2017). That is, resting-state modules become less differentiated as a function of increasing age.

Several previous studies have investigated the reconfiguration of functional brain connectivity, across resting and task states, in relation to adult age. Gallen et al. (2016), for example, used a blocked-design N-back task probing working memory and found that the reconfiguration of modules during the task, relative to rest, was greater in magnitude for older adults than for younger adults. During blocks with lower task demands (e.g., single-category vs. dual-category matching), between-module connectivity of lateral prefrontal regions was greater for older adults as compared to younger adults. Moreover, the increase in between-module connectivity in older adults was related to greater fractional anisotropy of the superior longitudinal fasciculus and faster task performance. Several other studies using various tasks and graph theoretical measures exhibit a similar trend, with increased functional connectivity among modules during a task relative to rest, more so in older as compared to younger adults (Chan et al. 2017; Grady et al. 2016; Hughes et al. 2020; Spreng et al. 2016; Zhang et al. 2021).

More generally, these findings suggest that network reconfiguration involves a decrease in system segregation, from rest to task states, which becomes more pronounced as a function of increasing age. This age-related pattern, however, has not been tested for system segregation specifically. Further, while choice discrimination tasks and related fluid cognitive abilities are the primary dimension of age-related cognitive decline (Madden 2001; Madden and Monge 2019; Salthouse 1985, 1996; Salthouse and Madden 2007), no previous study has investigated age-related reconfiguration of functional connectivity in the context of visual attention performance. Finally, limited evidence is available with regard to how graph theoretical measures of structural connectivity may contribute to age-related differences in the reconfiguration of functional connectivity (Gallen et al. 2016). Previous research suggests that age-related disconnection of white matter tracts leads to a loss of between-module structural connectivity, yielding a more locally organized network for older adults (Puxeddu et al. 2020; Wu et al. 2012; Zhao et al. 2015). In theory, structural connectivity should constrain functional connectivity (Damoiseaux and Greicius 2009; Fukushima et al. 2018; Honey et al. 2007, 2009), and some evidence suggests that age-related decline in functional connectivity is a response to declining structural network integrity (Andrews-Hanna et al. 2007; Fjell et al. 2016; Zimmermann et al. 2016). However, the strength of structure–function coupling may decrease with age (Betzel et al. 2014; Zamani Esfahlani et al. 2022), and other findings indicate that age may exert relatively independent effects on functional and structural connectivity (Fjell et al. 2017; Madden et al. 2020a; Pedersen et al. 2021; Schulz et al. 2022).

In this research we conducted graph theoretical analyses of age-related differences in resting-state functional, task-related functional, and structural connectivity, and the relation of these measures to an attention-demanding cognitive task: visual search. The identification of a visual target among nontarget items (distractors) is highly vulnerable to age-related decline, although some aspects of visual attention, such as top-down control and spatial selection, remain well preserved with age (Hommel et al. 2004; Kramer and Madden 2008; Madden 2007; Madden and Monge 2019; Rabbitt 2017). Merenstein et al. (2023) recently reported that age-related differences in the activation of frontoparietal brain regions during visual search were influenced by both the difficulty of target/distractor discrimination and the presence of an irrelevant feature (color singleton) in the visual display. Here, using the same sample of participants (68 healthy adults, 18–78 years of age), and additional imaging data (resting-state fMRI and DWI), we applied graph theoretical analyses to obtain estimates of functional and structural connectivity that were not included in the Merenstein et al. report. Thus, it was possible to investigate age-related differences in graph theoretical metrics for resting-state, task-related, and structural networks for the same individuals, as well as the relation of these measures to visual search performance.

Our first goal was to investigate age-related differences in functional system segregation, from the fMRI resting-state and task-related data, and in structural system segregation from the DWI data. We hypothesized that, overall, functional system segregation would decrease from rest to task, reflecting the increased connectivity among modules required for attentional allocation (Cohen et al. 2014; Spadone et al. 2015; Wen et al. 2015). We also expected to find an age-related decline in both resting-state system segregation (Chan et al. 2014; Deery et al. 2023; Wig 2017) and task-related system segregation (Chan et al. 2017; Gallen et al. 2016; Grady et al. 2016; Hughes et al. 2020; Spreng et al. 2016; Zhang et al. 2021). In contrast to the functional connectivity data, we hypothesized that system segregation for the structural connectivity data would increase as a function of age, on the basis of previous studies suggesting a differential loss of between-module structural connectivity for older adults (Puxeddu et al. 2020; Wu et al. 2012; Zhao et al. 2015).

The second goal was to determine the degree to which the different forms of functional and structural system segregation, as well as the functional reconfiguration between resting and task states, were related to age-related decline in visual search. We used the diffusion decision model of two-choice reaction time (Dutilh et al. 2019; Ratcliff and McKoon 2008; Ratcliff et al. 2016; Voss et al. 2013; Wagenmakers et al. 2007), to distinguish the rate of evidence accumulation (drift rate) from visual sensory encoding and motor processes (nondecision time) and cautiousness (boundary separation). From mediation and moderation analyses within ordinary linear regression (Agler and De Boeck 2017; Hayes 2013; Hayes and Rockwood 2017), we assessed the relative influence of functional and structural connectivity on the relation between age and visual search, focusing on those aspects of search performance exhibiting significant age-related effects.

We first included the resting-state, task-related, and structural forms of system segregation as parallel mediators of the relation between age and visual search performance, to determine if any of these network properties had a specific influence on age-related differences in visual search. Intuitively one might expect that task-related functional connectivity would have the most prominent influence, but previous evidence is not definitive on this point (Grady et al. 2016; Zhang et al. 2021), and few previous studies have directly compared resting-state and task-related functional connectivity, as predictors of cognitive performance. In view of the different components of visual information processing provided by the diffusion decision model, we expected that the different forms of system segregation would vary in their role as mediators or moderators, in relation to the specific behavioral outcomes of drift rate, nondecision time, and cautiousness. In separate analyses of the reconfiguration of functional connectivity, from resting to task states, we hypothesized that reconfiguration would increase with age, consistent with previous analyses of graph theoretical measures other than system segregation (Chan et al. 2017; Gallen et al. 2016; Grady et al. 2016; Hughes et al. 2020; Spreng et al. 2016; Zhang et al. 2021). We also expected that functional reconfiguration would have an influence on age-related differences in visual search performance. Finally, we examined the role of structural connectivity in relation to age, functional reconfiguration, and search performance. Our question here was whether the relation of reconfiguration, to age and visual search performance, could be characterized as a response to structural disconnection (Andrews-Hanna et al. 2007; Fjell et al. 2016; Zimmermann et al. 2016), or whether, alternatively, these functional and structural aspects of brain connectivity exhibited relatively independent effects of age (Fjell et al. 2017; Madden et al. 2020a; Pedersen et al. 2021; Schulz et al. 2022).

Materials and methods

Participants

The research was conducted in accordance with the Code of Ethics of the World Medical Association (Declaration of Helsinki) for experiments involving humans. Participants gave written informed consent for a protocol approved by the Duke University Medical Center Institutional Review Board. All participants were compensated for their time and completed an initial screening (Session 1); imaging was conducted approximately 1 month later in Session 2 (median days between sessions = 30). All participants reported that they had completed at least 12 years of education and were free of significant health problems, such as neurological disease, uncontrolled hypertension, or reliance on home oxygen (Christensen et al. 1992).

Screening tests for Session 1 included the Freiburg Visual Acuity test (Bach 1996), the Mini-Mental State Exam (MMSE; Folstein et al. 1975), the Beck Depression Inventory (BDI; Beck 1978), and the vocabulary subtest of the Wechsler Adult Intelligence Scale-III (WAIS-R; Wechsler 1997). Exclusion criteria were: visual acuity worse than 20/40 Snellen, a scaled score on the WAIS vocabulary subtest less than 10 (50th percentile), a MMSE score less than 27, or a BDI score greater than 15. Session 1 also included a computer-based practice version of the visual search task (360 trials) used in the task-related functional imaging for Session 2, and a battery of 12 neurocognitive computer-based tests of reaction time (RT) and standardized psychometric measures.

Ninety-eight community-dwelling individuals between 18 and 84 years of age completed Session 1. Nine participants were excluded based on the screening criteria. Two participants were outliers (> 3 SD) on one or more of the cognitive tests. Five participants were lost to recruitment for the MRI session, and four participants failed MRI safety screening (e.g., claustrophobia, body size, or metal implant). Seven participants were excluded for either excessive motion or low task performance during scanning (< 75% overall accuracy). Artifacts and technical issues with image processing further excluded three participants. The final sample (Table 1) comprised 68 participants (36 females), 18–78 years of age, who were comparable in years of education completed, MMSE, BDI, and WAIS vocabulary. The distribution of participants within each age decades was: 18–30 years ($n = 15$), 30s ($n = 13$), 40s ($n = 12$), 50s ($n = 8$), 60s ($n = 11$), and 70s ($n = 9$).

Age-related decline was evident in visual acuity, color vision, and tests of fluid cognition (Table 1). Merenstein et al. (2023) reported an analysis of the fMRI task-related activation, in relation to visual search performance during scanning, in this same sample of individuals. Here, we describe analyses of task-related functional connectivity, in relation to resting-state functional connectivity, structural connectivity, and visual search performance during scanning.

Visual search task

During the task-related runs, participants performed a two-choice version of visual search for T and F targets, with both feature search and conjunction search conditions, and color singleton display items that could correspond to either the target or one of the distractors. On each trial, a visual display of five items (one target and four distractors) was presented for 350 ms, and participants made a two-choice button-press response as to whether a normally oriented T or F target was present in the display. As illustrated in Fig. 1, the displays in each of six task conditions represented the combination of two search conditions (feature, conjunction), and three conditions for the presence of a color singleton (coinciding with either the target or a distractor, or not present in the display). In the feature search condition, the four distractors were all Os. In each conjunction search display, the four distractors comprised three different T–F hybrid characters, along with either a rotated T or a rotated F. Relative to feature search, conjunction search is a more difficult condition (i.e., decreased search efficiency) due to the greater featural similarity between targets and distractors (Madden 2007;

Table 1 Participant characteristics

Variable	*M* (*SD*)	Age correlation (*r*)	*p*
Education (years)	17.412 (2.294)	0.006	0.9607
MMSE	29.588 (0.604)	0.004	0.9719
BDI	2.647 (3.203)	0.077	0.5299
Vocabulary	58.529 (4.530)	−0.018	0.8858
Color vision	13.875 (0.476)	−0.253*	0.0375
Visual acuity (log MAR)	−0.009 (0.085)	0.355**	0.0030
General fluid cognition	0.0 (0.969)	−0.859***	0.0001
Perceptual speed	0.0 (0.947)	−0.808***	0.0001
Executive function	0.0 (0.795)	−0.784***	0.0001
Memory	0.0 (0.810)	−0.679***	0.0001

$n = 68$. Values are means, with standard deviations in parentheses; MMSE = raw score on Mini-Mental State Exam (Folstein et al. 1975); BDI = score on the Beck Depression Inventory (Beck 1978); Vocabulary = raw score on the vocabulary subtest of the Wechsler Adult Intelligence Scale III (WAIS; Wechsler 1997); Color Vision = score on Dvorine color plates (Dvorine 1963); Visual Acuity = logarithm of the minimum angle of resolution (MAR), for the Freiburg Visual Acuity Test (Bach 1996). Log MAR of 0 corresponds to Snellen 20/20, with negative values corresponding to better resolution. Thus, the positive correlation for acuity represents age-related decline in this measure. During Session 1, participants completed a battery of 12 neurocognitive computer-based tests of reaction time (RT) and standardized psychometric measures, comprising four tests for each of three domains of fluid cognition: perceptual-motor speed, executive function, and memory (Merenstein et al. 2023). The first factor from a factor analysis of all 12 tests was used as a measure of overall fluid cognition, and the first factor from each set of four tests for perceptual speed, executive function, and memory, was used as an indicator for each of these three cognitive domains. Factor score correlations with age are covaried for gender and WAIS vocabulary. Age correlations were not *FDR* corrected to provide a conservative estimate of age-related differences

*$p < 0.05$ (uncorrected)

**$p < 0.01$ (uncorrected)

***$p < 0.001$ (uncorrected)

Madden and Monge 2019; Wolfe and Horowitz 2004). For both types of search, displays with color singleton targets are expected to improve performance by enhancing target identification, whereas attentional capture from distractor singletons is expected to impair performance. Merenstein et al. (2023) provide additional details of the visual search task and outcome performance measures.

Participants performed 12 practice trials at the beginning of the MRI scanning in Session 2, during the susceptibility-weighted angiography (SWAN) structural imaging run. The final data set comprised the four event-related fMRI runs of 60 trials each (240 total test trials). Across the four runs, there were 40 trials (20 per T/F target) for each of the six task conditions (with the exception of two miscoded trials, identified and corrected during analyses). The 60 trials within each fMRI run contained 9–11 instances for each combination of search type and color singleton, distributed randomly. Participants were instructed to respond as quickly as possible without sacrificing accuracy. Feedback regarding response accuracy was provided during Session 1 but not during scanning.

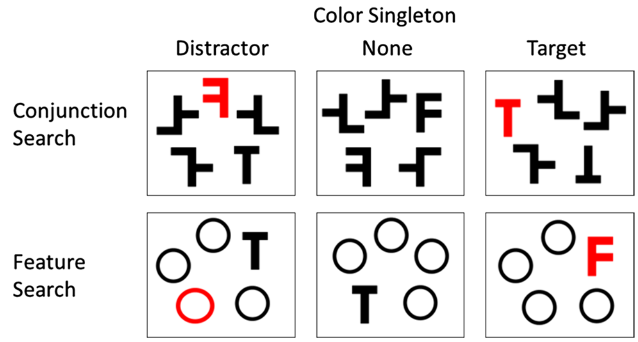

Fig. 1 Visual search task conditions. (Reproduced, with permission, from Merenstein et al. (2023). For interpretation of the references to color in this figure legend, the reader is referred to the Web version of this article.) Each display contained a target letter (T or F) and four nontarget (distractor) items. On each trial, participants made a two-choice decision regarding whether the T or F target was present in the display. In feature search, the distractors were always Os. In conjunction search, the distractors were rotated Ts and Fs and hybrid T–F characters. On two-thirds of the trials, one of the display items was a color singleton (a red item), which could be either the target or one of the distractors. The six different types of displays were presented in a random sequence within each fMRI run

Display presentation and response acquisition were controlled by a Windows-based PC running E-Prime 2.0 (Psychology Software Tools, Sharpsburg, PA, USA). Each trial began with a fixation cross with variable duration (jitter), followed by the search display for a duration of 350 ms, then a 2650 ms response screen, during which the display was white. We measured RT from display onset, allowing a total of 3000 ms for the response. Following the response period, the fixation cross returned to begin the next trial. The jitter duration was varied among values of 1500, 3000, 4500 ms, and 6000 ms defined by multiples of the fMRI repetition time (TR) value (1500 ms). The average jitter across trials was 3000 ms. The jitter values and trial order were distributed across conditions using the Optseq2 program (Dale 1999; https://surfer.nmr.mgh.harvard.edu/optseq/).

At the onset of each display, participants made a button-press response to indicate which target was present (T or F), using their right index and middle fingers resting on two buttons on a fiber optic response box (Current Designs, Philadelphia, PA, USA). We constructed two different sequential orders (forward and reverse) of the four blocks of test trials and combined those with the two assignments of the targets to the response buttons, to represent four test list versions, which were varied across participants.

Diffusion decision model for reaction time

The diffusion decision model estimates sensorimotor and decisional components of two-choice responses, in this case the T/F target identification, from the complete distributions of RT for correct and incorrect responses, and error rate (Ratcliff and McKoon 2008; Ratcliff et al. 2016; Voss et al. 2013). The model assumes that the decision on each trial is the result of evidence accumulation (drift rate; v) towards one of the two response boundaries, visual sensory and motor response processes (nondecision time; $t0$), and the participant's overall level of cautiousness (boundary separation; a). Here, we estimated these decisional components with the EZ-diffusion model (Wagenmakers et al. 2007). This method estimates fewer parameters than other methods, and is based on a mathematically simplified algorithm, but the EZ-diffusion model is as successful as more complex methods in recovering the underlying parameters (Dutilh et al. 2019; van Ravenzwaaij and Oberauer 2009). Data trimming criteria for the behavioral responses are described later in this Methods section (*Task-Related fMRI Processing*), and the sets of trials were identical for task-related functional connectivity and behavioral analyses, with the exception of the 78 high-motion trials deleted from the functional connectivity analyses. These latter trials were retained in the behavioral analyses as the RT values did not exceed the criteria for outliers.

MRI data acquisition

We collected all imaging data on a 3 T GE MR750 whole-body 60 cm bore MRI scanner (GE Healthcare, Waukesha, WI, USA) equipped with peak strength of 113 mT/m gradients and a 260 T/m/s slew rate. The scanner possessed an 8-channel head coil that was used for radio frequency (RF) reception. Participants wore earplugs to reduce scanner noise, and foam pads were used to minimize head motion. The scanning session comprised one run of T1-weighted anatomical images, one resting-state run of T2*-weighted (functional) imaging sensitive to the blood oxygen level dependent (BOLD) signal, one run of SWAN imaging, four runs of event-related T2*-weighted imaging, one run of diffusion-weighted imaging (DWI), and one run of T2-weighted fluid attenuated inversion recovery imaging (FLAIR). The SWAN and FLAIR data are not included in the present analyses.

Anatomical T1-weighted images included 292 straight axial slices that were attained using a 3D fast inverse-recovery-prepared spoiled gradient recalled (SPGR) sequence with TR = 2203.5 ms, echo time (TE) = 3.076 ms, inversion recovery time (TI) = 900 ms, field of view (FOV) = 240 mm^2, flip angle = 8°, voxel size = 0.47 × 0.47 × 0.5 mm, acquisition matrix = 512 mm^2, and a sensitivity encoding (SENSE) factor of 2.

The functional MRI (fMRI) scans, for both resting-state and task-related runs, were T2*-weighted gradient-echo, echo planar imaging (EPI) functional images. All fMRI runs were acquired as 50 contiguous slices at an axial oblique orientation, parallel to the plane connecting the anterior and posterior commissures (AC-PC plane), with TR = 1500 ms, TE = 30 ms, FOV = 256 mm^2, flip angle = 60°, voxel size = 2 mm isotropic, acquisition matrix = 128 mm^2, and a SENSE factor of 2. The resting-state run was collected with eyes open with central fixation and comprised a time-series of 300 brain volumes, collected over a period of 7.50 min. Participants completed four task-related runs. Each of the task-related runs were 264 brain volumes collected over 6.60 min.

The DWI data consisted of 92 contiguous slices acquired along the AC-PC plane using a spin-echo EPI pulse sequence, with TR = 4894 ms, TE = 64.7 ms, FOV = 220 mm^2, flip angle = 90°, voxel size = 1.5 mm isotropic, acquisition matrix size = 144 mm^2, and SENSE factor of 1. The DWI scan utilized 90 diffusion-encoding directions with two b values (1500 or 3000 s/mm^2) and two non-diffusion-weighted (b = 0 s/mm^2) shells. For 60 of the 68 participants (88% of the sample), a second diffusion sequence was acquired with six diffusion-weighted directions of opposite polarity using identical parameters, except that TR = 5260 ms.

Study-specific anatomical template

Connectivity measures for all imaging modalities—resting-state, task-related, and DWI—were obtained in a study-specific space. We created a study-specific anatomical template using the ANTs 2.3.3 (Advanced Normalization Tools; Avants et al. 2011) script for multivariate template construction. We used the output of the fMRIPrep v20.2.0 (Esteban et al. 2019) anatomical pipeline to skull-strip each participant's T1-weighted image and then averaged these 68 images to create an initial template. Each individual's T1-weighted image was then registered to the average template. The average transform from this step, along with a sharpening filter, were used to warp the template towards the true mean shape. These steps were repeated four times to yield the final study-specific template.

Resting-state fMRI processing

The image processing pipeline for the resting-state fMRI, task-related fMRI, and DWI data is illustrated in Fig. 2. We conducted preprocessing of the BOLD time-series data from the resting-state T2*-weighted (functional) images with fMRIPrep (Esteban et al. 2019) and xcpEngine v1.2.3

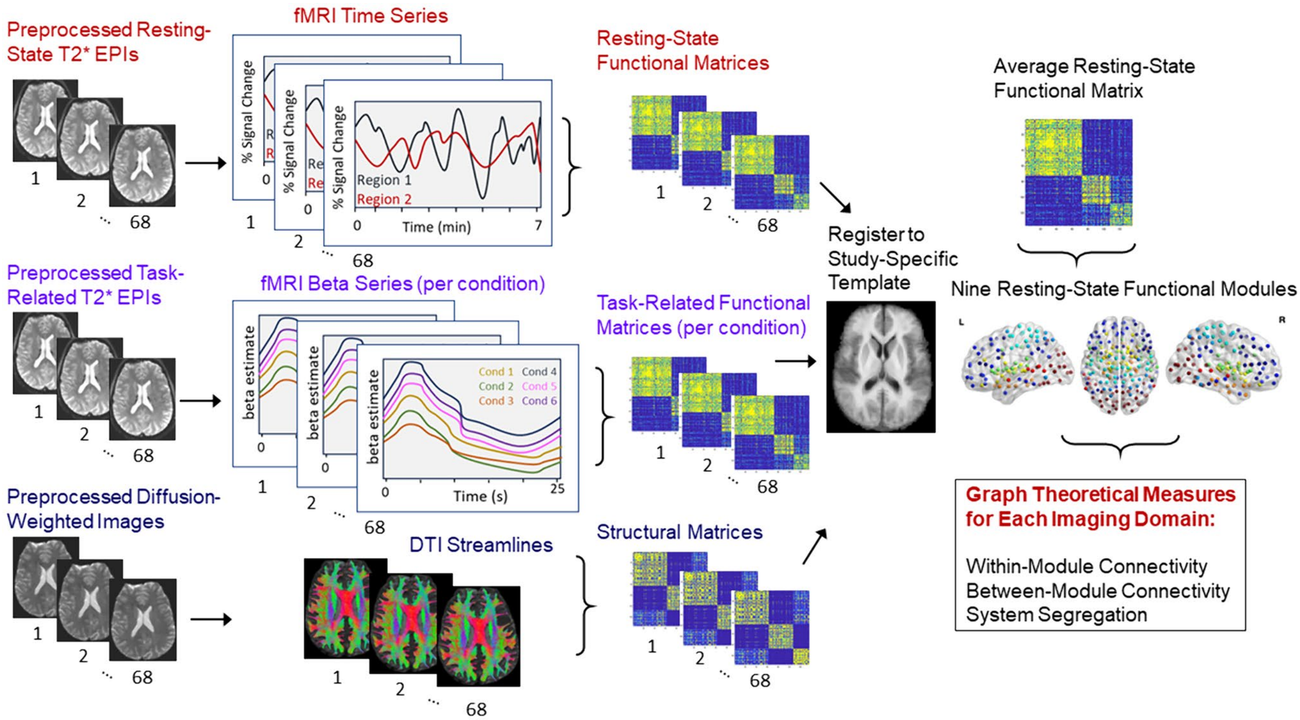

Fig. 2 Image processing pipeline. EPI, echo planar imaging; fMRI, functional magnetic resonance imaging; DTI, diffusion tensor imaging

(https://xcpengine.readthedocs.io/). Individual processing steps used tools from FSL v6.0.3 (FMRIB Software Library; Smith et al. 2004), AFNI v21.1.04 (Analysis of Functional NeuroImages; Cox and Hyde 1997), and ANTs.

Within fMRIPrep, the initial four volumes of the run were averaged to create a BOLD reference image, separately for each participant. This reference was registered to that participant's skull-stripped T1-weighted image using a boundary-based registration (Greve and Fischl 2009), to correct for susceptibility distortions in the absence of fieldmap images (Treiber et al. 2016). We then estimated head-motion parameters with respect to the BOLD reference (transformation matrices, and six corresponding rotation and translation parameters), before any spatiotemporal filtering, for subsequent confound regression. Slice timing correction was completed using AFNI *3dShift*; the corrected BOLD time-series was then resampled onto the participants' native space by applying a single, composite transform to correct for head motion and susceptibility distortions. Spatial smoothing was not performed, to avoid potential effects on functional network estimation (Alakörkkö et al. 2017).

We processed the fMRIPrep output with xcpEngine. The first four brain volumes were removed to ensure that the steady state equilibrium was attained. For confound regression, we included the six motion parameters and two physiological regressors (mean white matter [WM] signal and mean cerebral spinal fluid [CSF] signal), their temporal derivatives, and the quadratic expansions of the eight regressors and their temporal derivatives, yielding 32 nuisance regressors (Satterthwaite et al. 2013). These steps are equivalent to the Model 8 option (36 parameters plus motion scrubbing) described by Ciric et al. (2017), without the four parameters related to global signal regression (GSR). In some cases, GSR can improve data quality and assist in the detection of connectivity-behavior correlations (Ciric et al. 2017; Li et al. 2019). However, GSR can also create negative correlations in the resting-state fMRI correlation matrix, and it is not known whether negative correlations are biologically meaningful or a processing artifact (Murphy and Fox 2017; Ciric et al. 2018). Additional analyses of the present data incorporating the Chen et al. (2012) metric indicated that GSR would not reduce the level of noise. Thus, we chose not to include GSR in the fMRI processing pipeline. Finally, temporal band-pass filtering (0.01–0.08 Hz) was performed.

Mean framewise displacement (FD; Power et al. 2012) during the resting-state scans was 0.124 mm ($SD = 0.057$) before motion scrubbing and was correlated positively with age, $r = 0.274$, $p = 0.0237$. Before construction of resting-state functional connectivity correlation matrices (see the later section, *Functional and Structural Connectivity Estimation*), we performed motion scrubbing of resting-state volumes with > 0.50 mm using spectral interpolation. If fewer than five volumes remained between two outlier volumes, both outliers and all of the intervening volumes were scrubbed to account for residual motion (Power et al. 2014; Ciric et al. 2017; Parkes et al. 2018). Across participants, mean duration of the scrubbed resting-state data set was 7.29 min ($SD=0.270$), with a minimum of 5.75 min. Following motion scrubbing, the residualized image from xcpEngine was registered to the study-specific template using *antsRegistration.*

To assess resting-state functional connectivity, we created a single matrix of the correlations (Pearson r) of the resting-state fMRI timeseries data per node, for each participant. Because there is ambiguity regarding the interpretation of negative correlations, these were set to zero, as recommended by Rubinov and Sporns (2010). The matrix diagonal was also excluded from the calculations (i.e., set to not a number; NaN). We conducted analyses on undirected, weighted matrices, rather than on thresholded matrices, to retain sensitivity to this variation in connection strength (Rubinov and Sporns 2011). Finally, the matrix r values were transformed to Fisher z values.

Task-related fMRI processing

Initial processing of the task-related fMRI data was conducted within fMRIPrep in the same way as the resting-state fMRI data (as described in the previous section, *Resting-State fMRI Processing*) and then subjected to the same 32-parameter model for confound regression. As this specific set of 32 confound parameters is not an option provided by xcpEngine for task-related data, however, we instead manually constructed regression models for this set of confound parameters within FSL *FEAT* v6.0, the same tool called by the xcpEngine task module. Within *FEAT*, we removed non-brain tissue using *BET* (Brain Extraction Tool), applied grand-mean intensity normalization of the entire 4D dataset by a single multiplicative factor and high-pass temporal filtering (cut off = 90.0 s), and carried out time-series statistical analysis using *FILM* (FMRIB's Improved Linear Model) with local autocorrelation correction (Woolrich et al. 2001). Mean FD across all the volumes of the four task-related runs was 0.124 mm ($SD=0.061$), which did not differ significantly from resting-state FD, $t(67)=0.21$, $p=0.8378$, and was correlated positively with age, $r=0.382$, $p=0.0013$.

Analyses of the task-related data used a beta series approach (Cisler et al. 2014; Rissman et al. 2004), to define the parameter estimates of BOLD activation (betas) associated with the onset of the search display on each trial, within each of four task-related runs. Across all 68 participants, we excluded five runs (two runs for one participant and one run for each of three other participants), in which visual search accuracy was < 75%, leaving a total of 16,020 trial across all participants. We modeled each of these trials with a stick function (duration = 0) at display onset convolved with a double-gamma hemodynamic response function in FSL *FEAT*. We used a least squares separate (LSS) approach (Mumford et al. 2012), in which one explanatory variable modeled the regressor of interest, and a second explanatory variable modeled the remaining 59 trials within each run for each participant.

We first excluded 879 trials from the 16,020 total, where the target identification response was incorrect (5.49% of the total) and then excluded 17 of the remaining correct responses in which the RT was either < 250 ms or > 2500 ms (0.01%). To reduce the effect of motion, we identified 78 correct-response trials (0.516%) with FD > 1.0 mm, within a 6 s window, defined as 2 TRs (3 s) preceding and following display onset. The associated betas for these 974 incorrect, RT outlier, or high-motion trials were removed prior to constructing the connectivity matrices, leaving a total of 15,046 betas. Across the four runs, there was an average of 37 trials per participant ($SD=4$; minimum = 17), in each of the six task conditions.

To assess task-related functional connectivity, the betas for each task condition were used to construct separate undirected, weighted connectivity matrices for each condition for each participant: conjunction none, conjunction distractor, conjunction target, feature none, feature distractor, and feature target. We also combined all betas across the six trial types to estimate overall task connectivity for each participant. As with the resting-state data, negative correlations were set to zero and the matrix diagonal was excluded.

DWI processing

We processed the DWI data with MRtrix3 (http://mrtrix.org; Tournier et al. 2019), which also uses tools from FSL and ANTs. The DWI data were first de-noised (Veraart et al. 2016; Cordero-Grande et al. 2019) and then corrected for head motion, eddy currents, and susceptibility-induced distortions (Smith et al. 2004). Tissue-specific response functions were derived using the *dwi2response dhollander* algorithm. For the 60 participants with reverse polarity scans available, off-resonance field distortions were corrected using FSL *topup* (Andersson and Sotiropoulos 2016). We compared the quality control metrics derived from EddyQC between participants with and without the *topup* correction using independent sample t-tests. The two groups did not differ on signal-to-noise ratio, $p_{FDR}=0.716$, contrast-to-noise ratio, $p_{FDR}=0.716$, percentage of outlier volumes, $p_{FDR}=0.814$, or absolute motion, $p_{FDR}=0.814$ (FDR-corrected for four comparisons). Lastly, all data were bias-corrected using *dwibiascorrect* in MRtrix and non-brain tissue was removed to generate a whole-brain mask using *dwi2mask*. Absolute motion (calculated using eddy QC; Bastiani et al. 2019), with reference to the first $b=0$ volume, was 0.48 mm ($SD=0.10$) and relative, or framewise motion, was 0.15 mm ($SD = 0.05$). The correlation with age was not significant for either absolute motion, $p_{FDR} = 0.8185$, or relative motion, $p_{FDR} = 0.2048$ (FDR-corrected for two comparisons). The final, preprocessed DWI data were visually inspected and found to be acceptable for brain mask coverage, quality of motion and susceptibility-induced distortion correction, MR artifacts, and anatomical abnormalities.

The data for structural connectivity were obtained from Fiber Orientation Distribution (FOD) maps using multi-shell, multi-tissue constrained spherical deconvolution (Tournier et al. 2019). The tissue components within the FOD maps were normalized to correct for the effect of intensity inhomogeneities. We then generated streamlines using anatomically constrained probabilistic tractography (ACT; Smith et al. 2012), which limits the extent of streamline propagation and ensures proper termination of streamlines in the GM/WM interface. For each participant, 10 million tracts were generated using a minimum length of 250 mm and an FOD cutoff of 0.06 and then iteratively filtered to 1 million streamlines via spherical-deconvolution informed filtering of tractograms (*SIFT*; Smith et al. 2013). *SIFT* identifies false positive tracts that do not match the underlying white-matter anatomy via minimization of a cost-function based on the FOD (Yeh et al. 2016). These streamlines, however, are an indirect estimate of the underlying anatomy and are limited in several respects, for example a bias toward recovering more streamlines from shorter tracts (Guevara et al. 2020; Zhang et al. 2022). The endpoint of each streamline was assigned to the nearest GM node using a 4 mm radial search (Smith et al. 2015). The filtered streamlines for each participant were then transformed to the study-specific template.

To assess structural connectivity, we constructed symmetrical, unthresholded matrices, where each cell represents the total number of filtered streamlines connecting a pair of nodes, scaled to account for differences in node volume (Hagmann et al. 2008). As with the functional matrices, the matrix diagonal values were excluded. Note that although the T1 SPGR data are also structural data, the T1 data were used only for registration and construction of the study-specific anatomical template. When referring to structural connectivity, throughout this manuscript, we will be referring to the connectivity as estimated from the DWI data.

Network and node selection

The graph theoretical estimates of structural and functional connectivity begin from a predefined set of anatomical regions (nodes) and the connections among the nodes (edges) (Bullmore and Sporns 2009; Rubinov and Sporns 2010; Sporns 2011; Sporns and Betzel 2016). We used the Brainnetome Atlas (Fan et al. 2016) for node definition, which comprises 274 brain regions derived from probabilistic tractography using in vivo DWI data. However, we removed the 28 cerebellar nodes and 18 of the inferior temporal nodes because our MRI slice prescription for the T2*-weighted functional images did not sufficiently cover these regions. We transformed the final set of 228 anatomical nodes into the study-specific template space.

The properties of networks are difficult to compare directly when the network organization varies (van Wijk et al. 2010). Because a primary goal of this research was to investigate the reconfiguration of functional network organization from the resting state to the task-engaged state (and the relation to structural connectivity), we applied the same network parcellation, derived from the resting-state data, to all three imaging modalities, to provide a common ground for interpreting differences in the measures of connectivity. Thus, it is important to note that we are not attempting to characterize the individual modular structure for the different imaging modalities. Rather, we are measuring the connectivity within and between modules, for task-related functional and DWI structural data, for modules defined from the resting-state data.

To estimate a single parcellation of functional modules, we used the Brain Connectivity Toolbox (Rubinov and Sporns 2010) and input a group-averaged correlation matrix generated from the resting state fMRI data. Although several parcellations of resting-state fMRI data are available (Gordon et al. 2014; Ji et al. 2019; Power et al. 2011; Yeo et al. 2011), which would provide an independent definition of modular structure, these parcellations are based primarily on data from younger adults. In our view, the advantage of obtaining an accurate estimate of the modular structure for this particular data set, with individuals spanning the age range of 18–78 years, outweighed having an independent definition of the modules.

We estimated the data-driven, modular parcellation of the resting-state data by averaging the individual 228×228 functional connectivity matrices across all 68 participants. From this averaged connectome, we calculated the assignment of each of the 228 nodes to a specific module using 150 iterations of the Louvain algorithm (Blondel et al. 2008). We calculated the average agreement matrix across these 150 iterations, retaining values for only those pairs of nodes that were assigned to the same module for at least 50% of the iterations, and applied consensus clustering (Lancichinetti and Fortunato 2012) to obtain the group consensus modules.

Previously reported parcellations of resting-state functional connectivity from younger adult data typically comprise 7–17 functional modules (Gordon et al. 2014; Ji et al. 2019; Power et al. 2011; Yeo et al. 2011). We varied the spatial resolution parameter of the Louvain algorithm (gamma) across 15 values between 1.0 and 1.75 (Reichardt and Bornholdt 2006). The solution at gamma = 1.40 contained nine modules and was the only solution with seven or more modules that each included at least eight nodes. We therefore retained the nine-module parcellation, comprising frontoparietal, default mode, dorsal attention, sensorimotor, ventral attention, subcortical, limbic, frontotemporal, and visual modules. The modules are displayed in Fig. 3, and node-to-module assignments are listed in Supplementary Table S1. This nine-module parcellation, derived from group-averaged resting-state data, was then applied to the resting-state, task-related, and functional data.

As descriptive measures of the resting-state modular parcellation, we calculated *modularity* (Q) and *partition distance* (variation of information; VI), for each participant. Modularity refers to the degree to which the connections among all the nodes differ from a random structure (Newman and Girvan 2004), and partition distance refers to the degree to which two parcellations differ (Meilă 2007), in this case the difference between parcellation for an individual participant versus that of the group average. Age-related differences in the modularity of the network parcellation, and in the distance between the individual and group-averaged parcellation, were consistent across the selected range of 15 thresholds for spatial resolution (Supplementary Tables S2 and S3).

Graph theoretical measures

Here, we focused on *system segregation,* which is the ratio of within-module to between-module connectivity and reflects the degree to which modules are distinct or differentiated from each other (Chan et al. 2014; Wig 2017). Other graph theoretical measures, such as participation coefficient, are also sensitive to modular differentiation. Additional analyses (reported in Supplementary Material) of participation coefficient yielded results that were broadly similar to those obtained for system segregation. We calculated system segregation for the resting-state fMRI, task-related fMRI, and DWI data using custom MATLAB scripts. System segregation is defined by Eq. 1, where Z-within and Z-between are mean within- and between-module connectivity strength, respectively.

$$\textit{System segregation} = \left(\overline{Z}_{within} - \overline{Z}_{between}\right)/\overline{Z}_{within} \quad (1)$$

As noted in the Introduction, we also investigated the reconfiguration of functional connectivity, from resting to task states, in terms of the relative change in system segregation, expressed by Eq. 2, where Z-rest and Z-task are the average system segregation values for resting and task-related conditions, respectively. Reconfiguration can be viewed as the degree to which modules become more

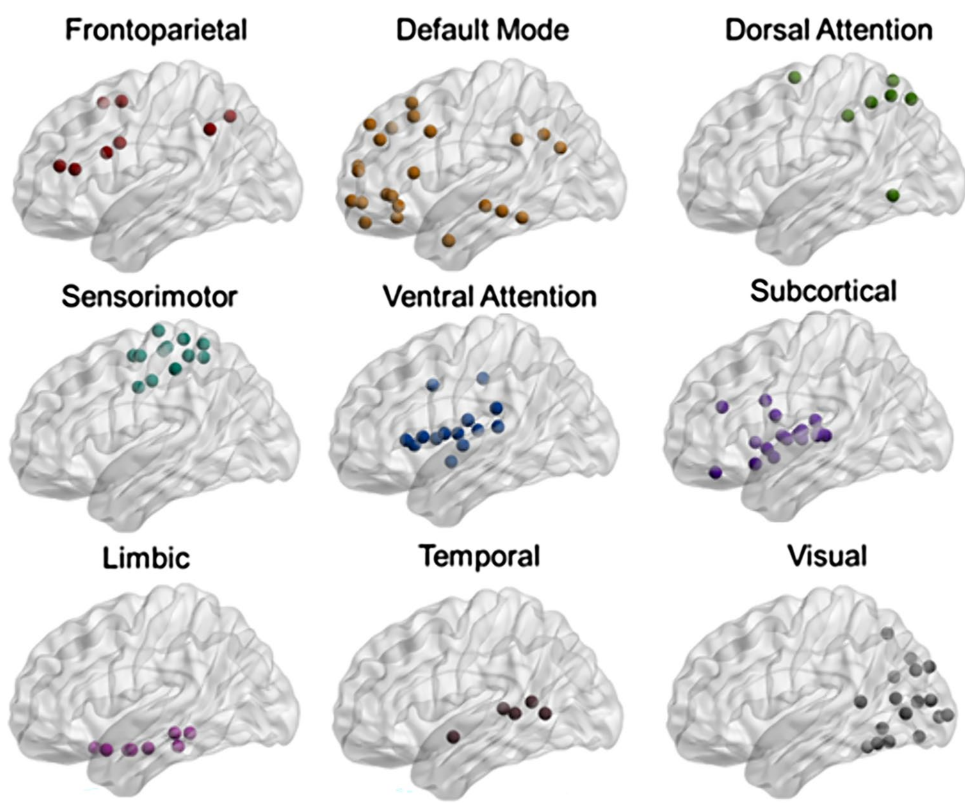

Fig. 3 Module parcellation. Nine data-driven modules were derived from group averaged resting-state fMRI data, using Brainnetome Atlas nodes (Fan et al. 2016) and the Brain Connectivity Toolbox (Rubinov and Sporns 2010), with the Louvain algorithm and consensus clustering, as described in the *Network and Node Selection* section of *Materials and Methods.* The nine modules were used for graph theoretical analyses of resting-state fMRI, structural, and task-related fMRI data

functionally integrated during the task, relative to the resting-state condition.

$$Reconfiguration = \left(\overline{Z}_{rest} - \overline{Z}_{task}\right)/\overline{Z}_{rest} \quad (2)$$

The estimation of connectivity, for both functional and DWI data, is influenced by motion (Ciric et al. 2017, 2018; Oldham et al. 2020; Power et al. 2012; Van Dijk et al. 2012). For each imaging domain (resting-state functional, task-related functional, and DWI), we thus included motion in that domain as a covariate in the analyses. Analyses of age-related effects for resting-state connectivity measures were covaried for mean FD during the resting-state scan, whereas task-related connectivity measures were covaried for mean FD across the four task-related runs. Analyses of the age-related effects for the DWI measures were covaried for mean relative (framewise) motion, which corresponds to the FD estimate from the fMRI data. Total intracranial volume, estimated using the standard FreeSurfer *recon-all* pipeline, was not included as a covariate, as preliminary analyses (reported in Supplementary Material) indicated that this variable did not vary significantly with age and did not account for significant age-related effects in the outcome variables.

Statistical analyses

All analyses were conducted within the general linear model, using repeated measures analysis of variance (ANOVA) to test the main effects and interactions of independent variables and Pearson's r correlation to test for the effects of age. Within a family of multiple comparisons, probability levels for statistical effects were corrected for the false discovery rate (FDR) with the Benjamini and Hochberg (1995) method. The individual table notes and figure legends state the number of comparisons for the individual familywise corrections. Regression models with visual search outcome measures included covariates for head motion for each of the imaging modalities represented in the model (as described in the previous paragraph) and visual acuity.

We investigated the role of the different forms of system segregation in age-related differences in visual search performance, using conditional process analyses of mediation and moderation, within ordinary linear regression (Agler and De Boeck 2017; Hayes 2013; Hayes and Rockwood 2017). A mediation effect is the interaction between variable paths, specifically between the path for the predictor to the mediator (the a path) and the path for the mediator to the outcome variable (the b path), controlling for the predictor. The total effect of the predictor on the outcome (the c path), comprises both an indirect effect (the $a \times b$ path interaction) and a direct effect (the c' path) that controls for the influence of the mediator as expressed in the ab interaction. Mediation effects, representing an influence of the mediating variable(s) on the relation between age and search performance, were considered significant if the bias-corrected 95% confidence intervals (CIs) did not contain zero, based on 10,000 bootstrap replacements within PROCESS macro (Hayes 2013). Note that the interpretation of a significant mediation effect (the $a \times b$ path interaction) does not rely on the presence of a significant total effect for the predictor variable, as the size of the total effect does not determine or constrain the size of the $a \times b$ path interaction (Hayes and Rockwood 2017). Moderation effects were tested by the interaction between age and mediator variable(s) in predicting the outcome measure.

Results

Diffusion decision model of visual search performance

Mean values of drift rate (v) and nondecision time ($t0$) parameters in each of the six task conditions are presented in Table 2, and the costs and benefits of the color singleton on search performance are presented in Table 3. Mean RT and accuracy for the task conditions are presented in Table S4. Note that increasing drift rate values represent a more efficient decision process (comparison of visual features), whereas increasing nondecision time values represent slower sensorimotor processing (visual encoding and response execution). The boundary separation parameter (a) is assumed to be constant across trials unless manipulated explicitly, and thus is measured across all trials without regard to task

Table 2 Search performance by task condition

Search condition	Singleton	*M* (*SD*)
Drift rate (v)		
Conjunction	Distractor	0.190 (0.049)
Conjunction	None	0.210 (0.053)
Conjunction	Target	0.254 (0.057)
Feature	Distractor	0.322 (0.067)
Feature	None	0.317 (0.079)
Feature	Target	0.300 (0.073)
Nondecision time ($t0$)		
Conjunction	Distractor	0.630 (0.113)
Conjunction	None	0.567 (0.090)
Conjunction	Target	0.518 (0.090)
Feature	Distractor	0.494 (0.077)
Feature	None	0.480 (0.083)
Feature	Target	0.470 (0.083)

$n = 68$. Drift rate and nondecision time values are means, with standard deviations in parentheses

Table 3 Costs and benefits of color singletons in conjunction search performance

Singleton effect	Mean (*SD*)	*t* (*SE*)	p_{FDR}
Drift rate (*v*)			
Distractor cost	0.073 (0.223)	2.68** (0.027)	0.0094
Target benefit	0.261 (0.345)	6.23*** (0.042)	0.0002
Nondecision time (t0)			
Distractor cost	0.114 (0.130)	7.25*** (0.016)	0.0001
Target benefit	0.080 (0.128)	5.16*** (0.016)	0.0001

$n=68$. Cost and benefit values were defined so that the resulting values would be primarily positive. For drift rate, Distractor Cost = (None − Dist)/None; Target Benefit = (Targ − None)/None. For nondecision time, Distractor Cost = (Dist − None)/None; Target Benefit = (None − Targ)/None. *t* value is difference from zero, FDR-corrected for two comparisons within each variable

*$p_{FDR} < 0.05$

**$p_{FDR} < 0.01$

***$p_{FDR} < 0.001$

condition. Merenstein et al. (2023) report complete analyses of the diffusion decision model parameters, including the costs and benefits of the color singleton on search performance. As discussed in that article, the primary findings in the search performance data were the following: Conjunction search was less efficient than feature search, as reflected in relatively lower drift rates and higher nondecision times for conjunction search. The color singleton influenced target discrimination, leading to more efficient target discrimination (higher drift rate and lower nondecision time) when the singleton corresponded to the target, and to less efficient discrimination when it corresponded to a distractor, relative to displays without a color singleton. The singleton effect, however, was evident only in the conjunction search condition. The color singleton did not influence highly efficient search in the feature condition.

In the present analyses of the relation between search performance and functional and structural connectivity, we focused on the three findings from the visual search performance data that exhibited age-related differences. First, cautiousness (boundary separation) increased with age, reflecting a more conservative decision threshold as a function of increasing age, $r=0.393$, $p=0.0010$ (covaried for visual acuity). Second, search efficiency (drift rate; v) decreased with age, but only in the conjunction search condition. The age correlations were $r=-0.367$, $p_{FDR}=0.0044$, for conjunction search, and $r=-0.113$, $p_{FDR}=0.363$, for feature search (covaried for visual acuity and FDR-corrected for two comparisons). These correlations differ significantly by Steiger's z (Steiger 1980), $z=2.592$, $p=0.0095$ (2-tailed). Thus, we analyzed the drift rate effect defined as the slowing for the conjunction search condition relative to feature search: (Feature − Conjunction)/Feature. Third, nondecision time increased with age, reflecting a slowing in visual encoding and motor response execution. The age-nondecision time correlations were $r=0.611$, $p_{FDR}<0.0001$, for conjunction search and $r=0.640$, $p_{FDR}<0.0001$, for feature search (covaried for visual acuity and FDR-corrected for two comparisons). Because the age-nondecision time correlations were comparable for feature search and conjunction search (Steiger's $z=-0.514$, $p=0.6072$, 2-tailed), nondecision time was averaged across the search conditions.

Functional and structural system segregation

For each participant's data within imaging modality (resting-state, task-related, and DWI), we first estimated each connectivity measure (system segregation, within-module connectivity, and between-module connectivity) separately for each module. We then averaged each estimate across the nine modules to obtain whole-brain (global) connectivity measures. In view of the relatively small variations in functional connectivity across the task conditions (see *Task Condition Effects* in Supplementary Material, and Supplementary Table S5), the outcome variable for task-related functional connectivity was the average across the task conditions, for each participant. Analyses of age-related effects included covariates for motion in the associated imaging domain.

Resting-state versus task-related effects

Global functional system segregation, calculated for each participant, was significantly higher for the resting-state data than for the task-related data, $t(67)=22.59$, $p<0.0001$ (Fig. 4, Panel A), reflecting a greater integration of modules during the task relative to rest. Comparison of resting-state versus task-related system segregation for each module individually indicated that system segregation was relatively higher in the resting-state for each module, with $t(67)>6.25$, $p_{FDR}<0.0001$ (corrected for nine comparisons), in each case.

To further characterize the change in system segregation from rest to task, we conducted a repeated measures ANOVA of the connectivity data, including global within versus between (connectivity type) and rest versus task (condition) as independent variables (Fig. 4, Panel B). The main effects for both connectivity type, $F(1, 67)=1273.74$, $p<0.0001$, $\eta_p^2=0.950$, and condition, $F(1, 67)=46.66$, $p<0.0001$, $\eta_p^2=0.411$, were significant. These main effects represent overall higher connectivity values for within-module connectivity relative to between-module connectivity, and higher connectivity for task relative to rest. The Connectivity Type × Condition interaction was also significant, $F(1, 67)=219.72$, $p<0.0001$, $\eta_p^2=0.766$, because within-module connectivity was essentially unchanged between rest

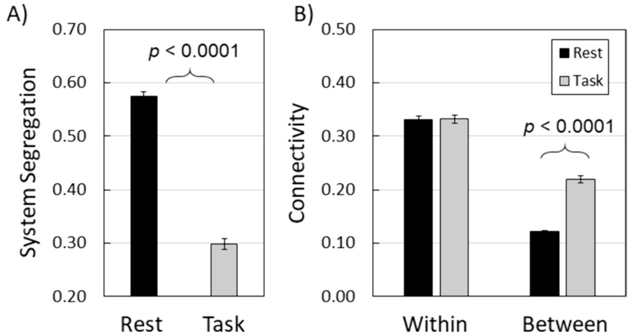

Fig. 4 Functional system segregation and within- versus between-module functional connectivity. Panel A = System segregation for resting-state and task conditions; Panel B = Within-module and between-module functional connectivity for resting-state and task conditions. Values are means (+/− SE), averaged across age

and task, $F(1, 67) = 0.03$, $p = 0.8577$, $\eta_p^2 = 0.001$, whereas between-module connectivity increased during the task relative to rest, $F(1, 67) = 224.84$, $p < 0.0001$, $\eta_p^2 = 0.770$.

Age-related effects

We first examined the age correlations for global system segregation in the two functional imaging domains. System segregation decreased significantly with age for both the resting-state data, $r = -0.450$, $p_{FDR} < 0.0001$, and task-related data, $r = -0.538$, $p_{FDR} < 0.0001$ (FDR-corrected for three comparisons, including the DWI data; Fig. 5, Panels A and B). The age-related decline in both forms of system segregation was due primarily to a decline in global within-module connectivity. The correlations of within-module connectivity with age for resting-state were $r = -0.322$, $p_{FDR} = 0.0136$, and for task were $r = -0.317$, $p_{FDR} = 0.0136$, whereas the age correlation for between-module connectivity was not significant for either rest ($r = 0.116$, $p_{FDR} = 0.4199$) or task ($r = 0.0189$, $p_{FDR} = 0.8796$; FDR-corrected for six comparisons, including the DWI data). In the resting-state data, the sensorimotor, ventral attention, frontotemporal, and visual modules exhibited significant age-related decline in system segregation (Table S6), whereas in the task-related data, the default mode, dorsal attention, ventral attention, and frontotemporal modules exhibited significant age-related decline in system segregation (Table S6).

In contrast to the resting-state and task-related functional data, global system segregation for structural connectivity *increased* significantly in relation to increasing age, $r = 0.415$, $p_{FDR} = 0.0050$ (Fig. 5, Panel C). The more pronounced age-related decline for global between-module connectivity ($r = -0.644$, $p_{FDR} = 0.0030$) relative to global within-module connectivity ($r = -0.455$, $p_{FDR} = 0.0030$; FDR-corrected for six comparisons) led to the age-related increase in structural system segregation. The age-related increase in structural system segregation was significant for the frontoparietal, ventral attention, subcortical, and visual modules, whereas the default mode module exhibited a significant decrease in structural system segregation (Table S6).

System segregation as a mediator of age-related differences in visual search performance

As noted previously in this Results section (*Diffusion Decision Model of Visual Search Performance*), we focused on the three findings from the visual search performance data that exhibited age-related differences: (a) the age-related increase in cautiousness (a; boundary separation); (b) the age-related slowing of drift rate (v) that was specific to conjunction search; and (c) the age-related slowing of nondecision time ($t0$). For each of these, we created a mediation model (Agler and De Boeck 2017; Hayes 2013; Hayes and Rockwood 2017) of the variables in which age was the predictor, search performance was the outcome, and different forms of system segregation were parallel mediators of the relation between age and search performance.

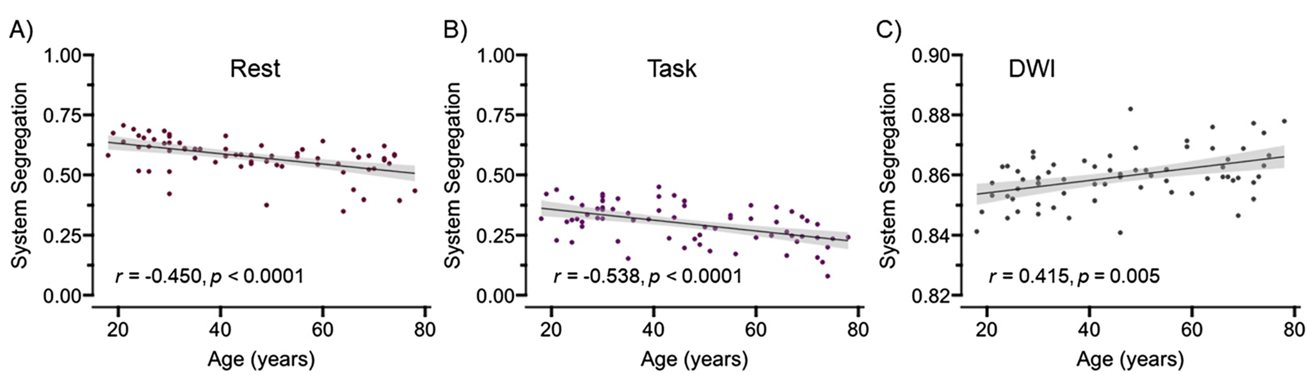

Fig. 5 System segregation as a function of age. Panel A = resting-state fMRI; Panel B = task-related fMRI; Panel C = diffusion-weighted imaging (DWI). Correlations are covaried for motion within each imaging domain and FDR-corrected for three comparisons

Cautiousness

Mediation analysis (Table 4) indicated that the variables of age, resting-state system segregation, task-related system segregation, and structural system segregation combined to account for 19.30% of the variance in cautiousness (boundary separation; *a*). None of the system segregation measures, however, had a mediating influence on the age-related increase in cautiousness. Similarly, moderation analyses indicated that none of the system segregation measures varied with age in the prediction of boundary separation. The Age × System Segregation interaction was $F(1, 62) = 0.10$, $p_{FDR} = 0.7572$, for resting-state system segregation, $F(1, 62) = 0.28$, $p_{FDR} = 0.7572$, for task-related system segregation, and $F(1, 62) = 0.13$, $p_{FDR} = 0.7572$, for structural system segregation (*FDR* corrected for three comparisons).

Conjunction search drift rate

Age and the three forms of system segregation accounted for 23.30% of the variance in the slowing of drift rate for conjunction search, relative to feature search (Table 5). In addition, resting-state system segregation was a mediator of the relation between age and conjunction search drift rate. The beta coefficient for the interaction was positive (β = 0.0011), reflecting the product of two negative effects: the decline in resting-state system segregation with increasing age (the *a* path), and the increase in the slowing of conjunction search drift rate with decreasing system segregation (the *b* path). Thus, age influenced the slowing of conjunction search drift rate indirectly, through the decrease in resting-state system segregation.

To confirm the mediation effect for resting-state system segregation, we rearranged the same predictor variables in a theoretically implausible, but statistically tractable model (Agler and De Boeck 2017; Salthouse 2011b), in which the relative slowing of conjunction search drift rate was a mediator of the relation between age and resting-state system segregation. In this model, conjunction search drift rate was not significant as a mediator, supporting the interpretation of resting-state system segregation as a mediator (Table 5).

With resting-state system segregation for each of the nine modules included as parallel mediators of the age-conjunction search drift rate relation, the default mode and sensorimotor modules made independent contributions as mediators (Table S7). Moderation analyses indicated that none of the three global system segregation measures varied with age in the prediction of the slowing of conjunction search drift

Table 4 Mediation of boundary separation (a) by system segregation

	Effect	*SE*	*t*	*p*	Lower CI	Upper CI
x = Age; m = Resting-state system segregation, Task-related system segregation, Structural system segregation; y = Boundary separation; covariates = resting-state motion, task-related motion, structural motion, visual acuity. $F(5, 62) = 2.96$, $p = 0.0186$, $r^2 = 0.193$						
Age effect (a path)						
Resting-state sys seg	**−0.0016**	**0.0005**	**−3.231**	**0.0020**	**−0.0026**	**−0.0006**
Task-related sys seg	**−0.0024**	**0.0005**	**−4.566**	**0.0000**	**−0.0035**	**−0.0014**
Structural sys seg	**0.0002**	**0.0001**	**3.835**	**0.0003**	**0.0001**	**0.0003**
Mediator to outcome (b path)						
Resting-state sys seg	0.0595	0.0392	1.520	0.1338	−0.0188	0.1379
Task-related sys seg	0.0273	0.0363	0.752	0.4554	−0.0454	0.1000
Structural sys seg	0.3457	0.3309	1.045	0.3005	−0.3165	1.0078
Total effect for age (c path)						
	0.0006	**0.0002**	**3.756**	**0.0004**	**0.0003**	**0.0009**
Direct effect for age (c' path)						
	0.0007	**0.0002**	**3.294**	**0.0017**	**0.0003**	**0.0011**
Mediation effect (a × b path interaction)						
Resting-state sys seg	−0.0001	0.0001	–	–	−0.0003	0.0000
Task-related sys seg	−0.0001	0.0001	–	–	−0.0003	0.0001
Structural sys seg	0.0001	0.0001	–	–	−0.0001	0.0003

$n = 68$. sys seg = system segregation; *a, b, c,* = paths in mediation model, with x (age) as the predictor variable, boundary separation (cautiousness) as the outcome variable (y), and resting-state system segregation, task-related system segregation, and structural system segregation as the mediators m; a = path from predictor to mediator; b = path from mediator to outcome, controlling for a path; c = total effect of predictor; c' = direct effect of predictor, controlling for mediator(s); ab = interaction of a and b paths representing indirect influence of x as mediated by m; effect = regression coefficient; SE = standard error; Lower/Upper CI = lower/upper bounds of bias-corrected 95% confidence intervals, estimated from bootstrap sampling with 10,000 samples. Significant effects are presented in bold

Table 5 Mediation of the relation of age to conjunction search drift rate by system segregation

	Effect	*SE*	*t*	*p*	Lower CI	Upper CI
x = Age; m = Resting-state system segregation, Task-related system segregation, Structural system segregation; y = Decrease in drift rate for conjunction search relative to feature search; covariates = resting-state motion, task-related motion, structural motion, visual acuity. $F(5, 62) = 3.77$, $p = 0.0048$, $r^2 = 0.233$						
Age effect (a path)						
Resting-state sys seg	**−0.0016**	**0.0005**	**−3.231**	**0.0020**	**−0.0026**	**−0.0006**
Task-related sys seg	**−0.0024**	**0.0005**	**−4.566**	**0.0000**	**−0.0035**	**−0.0014**
Structural sys seg	**0.0002**	**0.0001**	**3.835**	**0.0003**	**0.0001**	**0.0003**
Mediator to outcome (b path)						
Resting-state sys seg	**−0.6634**	**0.2356**	**−2.816**	**0.0066**	**−1.1349**	**−0.1920**
Task-related sys seg	0.1622	0.2185	0.742	0.4609	−0.2751	0.5994
Structural sys seg	1.0050	1.9912	0.505	0.6156	−2.9794	4.9894
Total effect for age (c path)						
	0.0015	0.0010	1.548	0.1268	−0.0004	0.0034
Direct effect for age (c' path)						
	0.0006	0.0012	0.488	0.6272	−0.0018	0.0030
Mediation effect (a × b path interaction)						
Resting-state sys seg	**0.0011**	**0.0006**	**–**	**–**	**0.0003**	**0.0025**
Task-related sys seg	−0.0004	0.0005	–	–	−0.0014	0.0005
Structural sys seg	0.0002	0.0004	–	–	−0.0006	0.0010
Feat − Conj Drift Rate	−0.0003	0.0002	–	–	−0.0009	0.0001

$n = 68$. sys seg = system segregation; feat = feature; conj = conjunction; *a, b, c,* = paths in mediation model, with x (age) as the predictor variable, and different variables for the outcome variable (y) and the mediator(s) m; a = path from predictor to mediator; b = path from mediator to outcome, controlling for a path; c = total effect of predictor; c' = direct effect of predictor, controlling for mediator(s); ab = interaction of a and b paths representing indirect influence of x as mediated by m; effect = regression coefficient; SE = standard error; Lower/Upper CI = lower/upper bounds of bias-corrected 95% confidence intervals, estimated from bootstrap sampling with 10,000 samples. Significant effects are presented in bold

rate relative to feature search. The Age × System Segregation interaction was $F(1, 62) = 0.17$, $p = 0.6798$, for resting-state system segregation, $F(1, 62) = 0.44$, $p = 0.6798$, for task-related system segregation, and $F(1, 62) = 1.92$, $p = 0.5115$, for structural system segregation (*FDR* corrected for three comparisons).

Nondecision time

A mediation model with age and the three forms of system segregation accounted for 30.90% of the variance in average nondecision time (Table 6). In this model, system segregation for the DWI structural data was a significant mediator of the relation between age and nondecision time. The beta coefficient for the interaction was positive ($\beta = 0.0005$), reflecting the increase in both structural system segregation as a function of age (the a path), and the increase in nondecision time with increasing system segregation (the b path). A model that reversed the roles of the predictors, designating nondecision time as a mediator of the relation between age and structural system segregation, did not yield significant mediation for nondecision time, confirming a specific, mediating role of structural system segregation in the relation between age and nondecision time. The increase in nondecision time with increasing age was thus an indirect effect (Table 6), reflecting the influence of increasing structural system segregation (i.e., anatomical separation of modules).

With structural system segregation for the nine modules included as parallel mediators of the age-nondecision time relation, none of the modules exhibited an independent effect as a mediator (Table S8). Moderation analyses indicated that none of the three global system segregation measures varied with age in the prediction of average nondecision time. The Age × System Segregation interaction was $F(1, 62) = 0.16$, $p = 0.4474$, for resting-state system segregation, $F(1, 62) = 2.20$, $p = 0.4302$, for task-related system segregation, and $F(1, 62) = 0.58$, $p = 0.4474$, for structural system segregation (*FDR* corrected for three comparisons).

Reconfiguration from rest to task

Functional reconfiguration

Across all participants, mean reconfiguration (Eq. 2) was 0.473 ($SD = 0.153$), which was significantly greater than zero, $t(67) = 25.54$, $p < 0.0001$, consistent with the reduction in system segregation for the task, relative to rest (see

Table 6 Mediation of the relation between age and nondecision time by system segregation

	Effect	*SE*	*t*	*p*	Lower CI	Upper CI
x = Age; m = Resting-state system segregation, Task-related system segregation, Structural system segregation; y = Average nondecision time; covariates = resting-state motion, task-related motion, structural motion, visual acuity. $F(5, 62) = 5.534$, $p = 0.0003$, $r^2 = 0.309$						
Age effect (*a path*)						
Resting-state sys seg	**− 0.0016**	**0.0005**	**− 3.231**	**0.0020**	**− 0.0026**	**− 0.0006**
Task-related sys seg	**− 0.0024**	**0.0005**	**− 4.566**	**0.0000**	**− 0.0035**	**− 0.0014**
Structural sys seg	**0.0002**	**0.0001**	**3.835**	**0.0003**	**0.0001**	**0.0003**
Mediator to outcome (*b path*)						
Resting-state sys seg	0.2147	0.1336	1.607	0.1133	− 0.0526	0.4820
Task-related sys seg	− 0.0516	0.1239	− 0.417	0.6785	− 0.2995	0.1963
Structural sys seg	2.0415	1.1288	1.809	0.0756	− 0.2173	4.3003
Total effect for age (*c path*)						
	0.0023	**0.0005**	**4.322**	**0.0001**	**0.0012**	**0.0033**
Direct effect for age (*c' path*)						
	0.0020	**0.0007**	**2.996**	**0.0040**	**0.0007**	**0.0034**
Mediation effect ($a \times b$ *path interaction*)						
Resting-state sys seg	− 0.0003	0.0003	–	–	− 0.0011	0.0002
Task-related sys seg	0.0001	0.0003	–	–	− 0.0004	0.0007
Structural sys seg	**0.0005**	**0.0003**	–	–	**0.0000**	**0.0011**

$n = 68$. sys seg = system segregation; *a, b, c,* = paths in mediation model, with x (age) as the predictor variable, and different variables for the outcome variable (y) and the mediator(s) m; a = path from predictor to mediator; b = path from mediator to outcome, controlling for a path; c = total effect of predictor; c' = direct effect of predictor, controlling for mediator(s); ab = interaction of a and b paths representing indirect influence of x as mediated by m; effect = regression coefficient; SE = standard error; Lower/Upper CI = lower/upper bounds of bias-corrected 95% confidence intervals, estimated from bootstrap sampling with 10,000 samples. Significant effects are presented in bold

Fig. 4, Panel A). The magnitude of the reconfiguration effect increased significantly with age (covaried for both resting FD and task FD), representing a greater functional integration of the modules, for the task relative to rest, with increasing age (Fig. 6). Analyses of the individual modules indicated that only the ventral attention module exhibited a significant age-related increase in reconfiguration (Table S9).

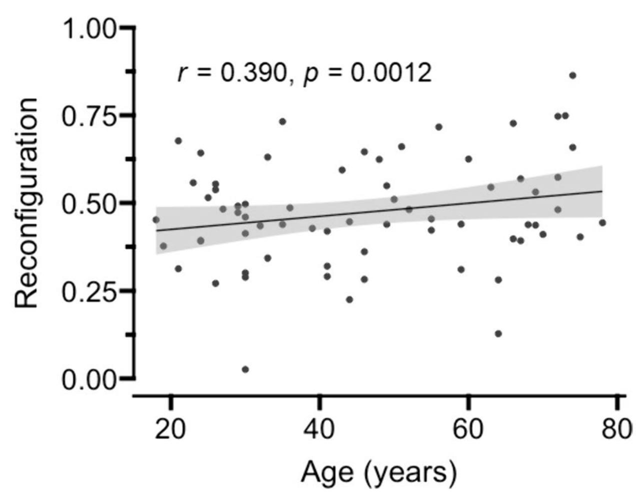

Fig. 6 Reconfiguration as a function of age. Reconfiguration is the relative decrease in functional system segregation for the task, relative to rest (defined by Eq. 2 in the text). Increasing reconfiguration represents an increase in the degree to which modules become more functionally integrated during the task, relative to the resting-state condition

Reconfiguration and search performance

When testing reconfiguration as a mediator of the relation between age and search performance, the mediation model accounted for 18.60% and 30.70% of the variance in cautiousness and nondecision time, respectively (Table 7, Models 1 and 2). However, reconfiguration did not have a mediating effect on age-related differences in either cautiousness or nondecision time. Tests for age moderation indicated that the interaction between age and reconfiguration, in predicting cautiousness and nondecision time, was not significant for either search performance variable. The Age × Reconfiguration interaction, with $F(1, 61)$, was 0.14, $p = 0.7060$, for cautiousness, and 0.72, $p = 0.3980$, for nondecision time.

The reconfiguration of system segregation between resting and task states was a significant mediator of the age-related slowing of conjunction search drift rate, relative to feature search (Table 7, Model 3). This model accounted for 23.30% of the variance in the relative slowing of conjunction search. The beta coefficient for the mediation effect

Table 7 Mediation of search performance by reconfiguration

	Effect	*SE*	*t*	*p*	Lower CI	Upper CI
Model 1: x = Age; m = Reconfiguration of system segregation from rest to task; y = Boundary separation; covariates = resting-state motion, task-related motion, visual acuity. $F(4, 63) = 3.60$, $p = 0.0105$, $r^2 = 0.186$						
Age effect (*a path*)						
Reconfig	**0.0029**	**0.0011**	**2.639**	**0.0105**	**0.0007**	**0.0051**
Mediator to outcome (*b path*)						
Reconfig	− 0.0042	0.0175	− 0.238	0.8125	− 0.0392	0.0308
Total effect for age (*c path*)						
	0.0006	**0.0002**	**3.774**	**0.0004**	**0.0003**	**0.0009**
Direct effect for age (*c' path*)						
	0.0006	**0.0002**	**3.630**	**0.0006**	**0.0003**	**0.0009**
Mediation effect ($a \times b$ *path interaction*)						
Reconfig	− 0.0000	0.0001	–	–	− 0.0001	0.0001
Model 2: x = Age; m = Reconfiguration of system segregation from rest to task; y = Average nondecision time; covariates = resting-state motion, task-related motion, visual acuity. $F(4, 63) = 6.98$, $p < 0.0001$, $r^2 = 0.307$						
Age effect (*a path*)						
Reconfig	**0.0029**	**0.0011**	**2.639**	**0.0105**	**0.0007**	**0.0051**
Mediator to outcome (*b path*)						
Reconfig	0.0326	0.0602	0.541	0.5904	− 0.0877	0.1529
Total effect for age (*c path*)						
	0.0023	**0.0005**	**4.354**	**0.0001**	**0.0012**	**0.0033**
Direct effect for age (*c' path*)						
	0.0022	**0.0006**	**3.937**	**0.0002**	**0.0011**	**0.0033**
Mediation effect ($a \times b$ *path interaction*)						
Reconfig	0.0001	0.0002	–	–	− 0.0002	0.0006
Model 3: x = Age; m = Reconfiguration of system segregation from rest to task; y = Feat – Conj Drift Rate; covariates = resting-state motion, task-related motion, visual acuity. $F(4, 63) = 4.79$, $p = 0.0019$, $r^2 = 0.233$						
Age effect (*a path*)						
Reconfig	**0.0029**	**0.0011**	**2.639**	**0.0105**	**0.0007**	**0.0051**
Mediator to outcome (*b path*)						
Reconfig	− 0.1627	0.1067	− 1.526	0.1322	− 0.3760	0.0505
Total effect for age (*c path*)						
	0.0015	0.0009	1.560	0.1237	− 0.0004	0.0034
Direct effect for age (*c' path*)						
	0.0020	0.0010	1.977	0.0525	− 0.0000	0.0039
Mediation effect ($a \times b$ *path interaction*)						
Reconfig	**− 0.0005**	**0.0003**	–	–	**− 0.0013**	**− 0.0000**

$n = 68$. Reconfig = reconfiguration of system segregation from rest to task; Feat – Conj Drift Rate = slowing of conjunction search drift rate relative to feature search; *a, b, c,* = paths in mediation model, with x (age) as the predictor variable, and different variables for the outcome variable (y) and the mediator(s) m; a = path from predictor to mediator; b = path from mediator to outcome, controlling for a path; c = total effect of predictor; c' = direct effect of predictor, controlling for mediator(s); ab = interaction of a and b paths representing indirect influence of x as mediated by m; effect = regression coefficient; SE = standard error; Lower/Upper CI = lower/upper bounds of bias-corrected 95% confidence intervals, estimated from bootstrap sampling with 10,000 samples. Significant effects are presented in bold

was negative (β = − 0.0005), as a result of the multiplicative effect of the relation between the positive age-reconfiguration path and the negative (but nonsignificant) reconfiguration-search performance path. That is, controlling for age, those individuals with greater reconfiguration of system segregation, from rest to task, exhibited less slowing of conjunction search drift rate relative to feature search. In addition, testing an alternative model, with conjunction search drift rate as a mediator of the age-reconfiguration relation, did not yield a significant mediation effect, supporting the interpretation of reconfiguration as a mediator of the age-search performance relation. The beta coefficient for conjunction search drift rate as a mediator, in this alternative model, was − 0.003 (SE = 0.0003; 95% Lower/Upper CI = − 0.0013/0.0001).

With reconfiguration for the nine modules included as parallel mediators of the age-related slowing of conjunction search drift rate, none of the modules exhibited an independent effect as a mediator (Table S10). A moderation test did not yield significant interaction between age and reconfiguration in the prediction of conjunction search drift rate, $F(1, 61) = 0.17$, $p = 0.6781$.

Structural disconnection and functional reconfiguration

To what extent is functional reconfiguration a response to the age-related increase in the structural separation of modules, as indicated by the age-related increase in structural system segregation (Fig. 5, Panel C)? Because reconfiguration was a mediator of the age-related decline in conjunction search drift rate (Table 7, Model 3), we explored a model in which both structural system segregation and reconfiguration were mediators of the relation between age and conjunction search drift rate. The two mediators were arranged in serial, such that structural system segregation was influencing reconfiguration (Table 8, Model 1). This model accounted for 23.30% of the variance in the slowing of conjunction search drift rate, relative to feature search. Reconfiguration remained significant as a mediator of the age-search performance relation. Structural system segregation, however, did not exhibit a significant relation to either reconfiguration or conjunction search drift rate.

When tested individually, structural system segregation was not correlated with functional reconfiguration (covaried for motion), $r = 0.055$, $p = 0.6647$. Age was not a moderator in regression models (with motion covariates) of the relation between structural system segregation and functional system segregation, for either rest, $F(1, 62) = 0.17$, $p = 0.6845$, or task, $F(1, 62) = 0.06$, $p = 0.8059$.

Discussion

In this research we brought graph theoretical analyses to bear on data comprising resting-state and task-related functional connectivity, structural connectivity, and cognitive task performance (visual search), for 68 healthy adults sampled continuously from 18 to 78 years of age (Merenstein et al. 2023). Using a modular parcellation derived from the participants' resting-state data (Figs. 1 and 2), we addressed

Table 8 Structural system segregation and functional reconfiguration as serial mediators of search performance

	Effect	SE	t	p	Lower CI	Upper CI
x = Age; m = Structural system segregation → Reconfiguration of system segregation from rest to task; y = Feat – Conj Drift Rate; covariates = resting-state motion, task-related motion, structural motion, visual acuity. F(5, 62) = 3.77, p = 0.0048, r^2 = 0.233						
Age effect (a path)						
Structural sys seg	**0.0002**	**0.0001**	**3.835**	**0.0003**	**0.0001**	**0.0003**
Reconfig	**0.0032**	**0.0012**	**2.775**	**0.0073**	**0.0009**	**0.0056**
Mediator to outcome (b path)						
Structural sys seg	1.0121	2.0664	0.490	0.6261	− 3.1212	5.1455
Reconfig	− 0.1823	0.1160	− 1.572	0.1213	− 0.4142	0.0497
Total effect for age (c path)						
	0.0015	0.0010	1.548	0.1268	− 0.0004	0.0034
Direct effect for age (c' path)						
	0.0018	0.0011	1.595	0.1160	− 0.0005	0.0040
Mediation effect (a × b path interaction)						
Structural sys seg	0.0002	0.0004	–	–	− 0.0006	0.0011
Structural sys seg → Reconfig	0.0001	0.0001	–	–	− 0.0001	0.0004
Reconfig	**− 0.0006**	**0.0004**	–	–	**− 0.0017**	**− 0.0001**

n = 68. Reconfig = reconfiguration of system segregation from rest to task; Structural sys seg = DWI structural system segregation; Feat – Conj Drift Rate = slowing of conjunction search drift rate relative to feature search; *a, b, c,* = paths in mediation model, with *x* (age) as the predictor variable, and different variables for the outcome variable (*y*) and the mediators (*m*); *a* = path from predictor to mediator; *b* = path from mediator to outcome, controlling for *a* path; *c* = total effect of predictor; *c'* = direct effect of predictor, controlling for mediator(s); *ab* = interaction of *a* and *b* paths representing indirect influence of *x* as mediated by *m*; effect = regression coefficient; SE = standard error; Lower/Upper CI = lower/upper bounds of bias-corrected 95% confidence intervals, estimated from bootstrap sampling with 10,000 samples. Significant effects are presented in bold two major aims: (a) age-related differences in functional and structural brain connectivity, especially system segregation, and (b) the relation of these measures of brain connectivity, including the reconfiguration of functional network connectivity, between resting and task-related states, to age-related differences in visual search performance.

Functional and structural connectivity

The results replicated several findings relevant to the first goal, starting from the changes in functional connectivity between resting and task-related states. Across the sample as a whole, we observed a decrease in system segregation from rest to task (Fig. 4, Panel A), as hypothesized, consistent with the increased integration of modules necessary to support the attentional demands of task performance (Braun et al. 2015; Cohen and D'Esposito 2016; Cohen et al. 2014; Elton and Gao 2015; Shine et al. 2016; Spadone et al. 2015; Wen et al. 2015). This task-related decrease in system segregation was significant for each of the nine modules.

What is not widely emphasized in the literature to date is that because system segregation is a relative measure, indexing the strength of within-module connectivity relative to between-module connectivity (Eq. 1), different patterns of change, for within- and between-module connectivity, may yield comparable levels of change in system segregation across resting and task-related states. In studies of younger adults, for example, Cohen et al. (2014) and Spadone et al. (2015) observed, as we do here, that modules are more interconnected during a task than in the resting state. Both of these previous studies, however, describe task-related reconfiguration as involving both a decrease in within-module connectivity and an increase in between-module connectivity. Our findings, in contrast, indicate that within-module functional connectivity was essentially unchanged between rest and task, with the task-related decrease in system segregation being due entirely to the increase in between-module connectivity occurring during the task (Fig. 4, Panel B). Thus, comparable changes in system segregation may reflect different combinations of within- and between-module connectivity, which in turn may reflect variation, across studies, in demographic variables (e.g., age range) and task demands (e.g., visual target discrimination vs. working memory).

The age-related decline in resting-state system segregation is well established (Chan et al. 2014; Deery et al. 2023; Goh 2011; Madden et al. 2020a; Malagurski et al. 2020; Ng et al. 2016; Pedersen et al. 2021; Wig 2017) and confirmed here (Fig. 5, Panel A). Analyses of the individual modules suggested that the age-related decline was most pronounced for the sensorimotor, ventral attention, frontotemporal, and visual modules (Table S6), which was unexpected in view of the proposal that age-related decline in resting-state system segregation is greater in magnitude for modules associated with higher-order, cognitive functions, relative to sensorimotor modules (Chan et al. 2014; Malagurski et al. 2020; Pedersen et al. 2021). Other findings, however, have also reported age-related decline in the functional segregation of sensorimotor modules (He et al. 2012; Roski et al. 2013).

The age-related decline in system segregation for task-related functional connectivity during visual search (Fig. 5, Panel B), is consistent with previous investigations of other tasks, particularly different versions of working memory (Chan et al. 2017; Gallen et al. 2016; Grady et al. 2016; Hughes et al. 2020; Spreng et al. 2016; Zhang et al. 2021). Interestingly, the age-related declines in both resting-state and task-related functional connectivity were due entirely to age-related decline in within-module connectivity, whereas the overall change in system segregation from rest to task, when averaged across the age variable, was the result of increased between-module functional connectivity (Fig. 4, Panel B). This is surprising because age-related increases in between-module connectivity have been observed for both resting-state (Chan et al. 2014) and task-related (Gallen et al. 2016) analyses. The between-module increase would be expected if older adults' increased correlations among modules reflected a modification of network structure in response to diminishing attentional resources (Chan et al. 2017; Gallen et al. 2016; Hughes et al. 2020; Spreng et al. 2016). While the reason for the differences across studies is not clear, Deery et al. (2023) noted in their review of the resting-state literature, that age-related decrease in within-module connectivity was more prominent (72% of studies) than age-related increase in between-module connectivity (54% of studies).

The age-related increase in structural system segregation in these data (Fig. 5, Panel C), as hypothesized, is consistent with the age-related disconnection of white matter pathways (Bennett and Madden 2014; Salat 2011), leading to a more locally organized structural network for older adults (Puxeddu et al. 2020; Wu et al. 2012; Zhao et al. 2015). In this case, whereas both within-module and between-module structural connectivity decreased with age, the age-related decrease was more pronounced for between-module connectivity, leading to increased segregation of the modules. The increased modular segregation was evident for the frontoparietal module, as well the ventral attention, subcortical, and visual modules (Table S6). Related findings from conventional diffusion tensor imaging studies (Wu et al. 2016) suggest that age-related differences in white matter microstructure are greater for long-range white matter pathways, contributing to between-module connectivity, as compared to more superficial white matter. A combination of various neurobiological mechanisms, including age-related decreases in myelination (Bartzokis 2004; Sams 2021) and increases in white matter hyperintensity volume (Tuladhar et al. 2016; Lu et al. 2024; Du et al. 2021) likely contribute to the increased segregation of structural modules.

Functional reconfiguration, structural connectivity, and visual search performance

The visual search behavioral data (Table 2) yielded three prominent age-related differences in parameters of the drift diffusion model (Dutilh et al. 2019; Merenstein et al. 2023; Ratcliff et al. 2016): (a) an age-related increase in cautiousness; (b) an age-related slowing of the rate of visual evidence accumulation (drift rate), which was specific to the more difficult task condition (conjunction search; Fig. 1); and (c) an age-related slowing in sensorimotor processing (nondecision time), which was relatively constant across the various task conditions. The presence of a color singleton in the display had both positive and negative influences on target discrimination, in the conjunction search condition, depending on the coincidence of the singleton with the target (Dent 2023; Theeuwes 2010; Wöstmann et al. 2022; Yantis 1996), but the singleton effects were constant with age (Table 3). This pattern is consistent with previous behavioral studies of aging using the diffusion decision model, which have yielded reliable age-related increases in nondecision time and cautiousness (Madden et al. 2020b; Ratcliff 2008; Servant and Evans 2020). The age-related slowing of the drift rate parameter is more variable and appears to require a level of task complexity, as in the conjunction search condition.

In addressing our second goal, identifying the relation of network connectivity to age-related decline in visual search performance, we found that functional and structural system segregation, as well as the functional reconfiguration between resting and task states, had specific influences on age-related differences in the different components of visual search. Comparing the three forms of system segregation as mediators of the relation between age and visual search performance, we found that the age-related increase in cautiousness was independent of functional and structural system segregation (Table 4). However, resting-state system segregation emerged as a significant mediator of the age-related decline in the efficiency of visual evidence accumulation for conjunction search (Table 5), with specific contributions from the default mode and sensorimotor modules (Table S7). Mediation was not significant when we rearranged the causal order of the predictor variables (Agler and De Boeck 2017; Salthouse 2011b), providing additional support that the observed mediation was interpretable. It is surprising that the resting-state measure outperformed task-related system segregation (Geerligs et al. 2014; Madden et al. 2010; Monge et al. 2017), as a mediator, but several previous studies have noted correlations between various forms of resting-state functional connectivity and age-related differences in composite, psychometric measures of cognition (Chan et al. 2014; Pedersen et al. 2021; Madden et al. 2017b, 2020a), and we have previously observed resting-state measures to be correlated with age-related differences in visual search (Madden et al. 2017a).

The age-related increase in nondecision time represents the combined effects of relatively early, sensory-level encoding and later, motoric processes of the button-press response. These encoding and response processes are common to all the task conditions. Similarly, the age-related increase in nondecision time was constant across the task conditions, reflecting a generalized, age-related slowing in these encoding and response processes (Madden 2001; Madden and Monge 2019; Salthouse 1985, 1996; Salthouse and Madden 2007). Mediation analyses indicated that structural system segregation was significant as a mediator of the age-related slowing of nondecision time (Table 6). As with the functional mediation analyses, rearranging the order of predictor variables supported the validity of structural system segregation as a mediator. Although various aspects of brain structure, particularly white matter microstructure, correlate with age-related decline in fluid cognition (Bennett and Madden 2014; Bennett et al. 2012; Madden et al. 2020a, b; Salami et al. 2012), previous evidence for specific influences of brain structure on age-related differences in cognition is not strong (Salthouse 2011b). The present findings suggest that structural and resting-state functional system segregation have distinct influences in our visual search task: Whereas resting-state functional system segregation contributes to age-related decline in the more cognitive component of the rate of information extraction (especially in conjunction search), structural system segregation influences age-related slowing of the more sensorimotor processes that are independent of the decision process (Rabbitt et al. 2007; Bendlin et al. 2010; Salami et al. 2012).

Finally, the decrease in functional system segregation for the task, relative to rest, as reflected in our measure of reconfiguration (Eq. 2), increased with age, as hypothesized (Fig. 6). That is, the age-related decrease in the segregation of modules (driven primarily by decreased within-module connectivity) is not just associated with resting and task states when considered individually, but is evident as a further decrease in functional system segregation during the task, relative to rest. We propose that this age-related increase in functional reconfiguration (Fig. 6) represents the increased integration of functional modules required by the attentional demands of visual target discrimination, in line with working memory and other forms of fluid cognition (Chan et al. 2017; Gallen et al. 2016; Grady et al. 2016; Hughes et al. 2020; Spreng et al. 2016; Zhang et al. 2021). Further, the reconfiguration of system segregation between resting and task states was a significant mediator of the age-related slowing of conjunction search drift rate, relative to feature search (Table 7, Model 3), consistent with the related effect observed in the resting-state data (Table 5).

Although we had expected that age-related differences in structural system segregation would constrain the influence of functional reconfiguration (Andrews-Hanna et al. 2007; Fjell et al. 2016; Zimmermann et al. 2016), this was not the case (Table 8). Similarly, the correlations between the structural and functional connectivity measures were not significant. This pattern may be consistent with a weakening of structural–functional relation with age (Betzel et al. 2014; Zamani Esfahlani et al. 2022), but the weakening was not sufficiently prominent to be expressed as an age moderation of the relation between structural and functional connectivity. In this visual search task, the influence of structural connectivity on age-related differences in nondecision time, and the influence of functional connectivity on age-related differences in the efficiency of evidence accumulation, appear to be relatively independent age-related effects (Fjell et al. 2017; Madden et al. 2020a; Pedersen et al. 2021; Schulz et al. 2022).

Limitations

In these analyses of functional and structural system segregation, we applied the modular parcellation defined from our resting-state data, at a particular spatial resolution (gamma = 1.40) to the task-related and structural data. Analyses at different levels of spatial resolution, or with different parcellations (Gordon et al. 2014; Ji et al. 2019; Power et al. 2011; Yeo et al. 2011), may yield different results (Arslan et al. 2018; Zalesky et al. 2010). In addition, the measure of structural connectivity in our analyses is derived from the estimated number of streamlines between two nodes, which is an indirect estimate that may not agree with the true underlying neuroanatomy (Guevara et al. 2020; Zhang et al. 2022). Finally, we compared network organization derived from timeseries analysis during the resting state to that derived from beta-series analysis during the task. These estimates are thus arising from different physiological properties of the BOLD signal (i.e., background connectivity during rest versus evoked connectivity during task). We believe, however, that the advantage of providing a common metric for the observed differences across imaging modalities outweighs these particular limitations. Similarly, we have focused primarily on system segregation, out of a wide variety of graph theoretical measures characterizing the features of brain networks (Bullmore and Sporns 2009; Rubinov and Sporns 2010; Sporns 2011; Sporns and Betzel 2016), as a first step in establishing the fundamental relations among the resting-state, task-related, and structural data. Current theories of age-related differences in functional connectivity have featured system segregation as a useful measure for summarizing age-related differences in connectivity within and between modules (Chan et al. 2014; Madden et al. 2020a; Wig 2017), but additional analyses of related measures (e.g., participation coefficient) will provide complementary information.

The analyses were also limited to characterizing the patterns of shared and unique variance in the outcome measures, within ordinary linear regression of cross-sectional data. We thus emphasize that the present results, including the mediation effects (Agler and De Boeck 2017; Hayes 2013; Hayes and Rockwood 2017), refer to differences among individuals in relation to chronological age, not change over time as would be measured from a longitudinal design (Hofer and Sliwinski 2001; Lindenberger et al. 2011; Maxwell and Cole 2007). However, the age-related decline in resting-state system segregation, observed here, is also evident in longitudinal investigations (Ng et al. 2016; Pedersen et al. 2021). The cross-sectional design avoids the blurring in the estimation of age-related variance, from practice effects, which can occur in longitudinal designs (Salthouse 2011a; Salthouse and Nesselroade 2002).

Conclusions

In this graph theoretical analysis, using the same modular parcellation across functional and structural brain connectivity data, we obtained age-related decline in resting-state and task-related functional system segregation, and age-related increase in structural system segregation, consistent with previous findings. Thus, whereas functional connectivity becomes more globally organized with increasing age, structural connectivity becomes more locally organized. Further, the reconfiguration of functional system segregation, from the resting to task state, increased with age, presumably in support of the attentional demands of visual target discrimination. Functional and structural system segregation also exhibited qualitatively different influences on visual search performance: Functional system segregation (including reconfiguration) influenced the age-related slowing in the rate of evidence accumulation, whereas structural system segregation contributed to the age-related slowing of nondecisional (encoding and response) processes. However, within this form of visual search, and these measures of brain connectivity, the age-related increase in functional reconfiguration does not appear to be a direct response to a corresponding decline in structural connectivity.

Supplementary Information The online version contains supplementary material available at https://doi.org/10.1007/s00429-024-02807-2.

Acknowledgements We are grateful for assistance from Angela Cook, Amalia Desir, Cortney Howard, Zach Monge, Alexa Putka, Nicole Stepovich, Ragini Singh, Chidi Ugonna, and Tina Zhao.

Author contributions DJM was responsible for conceptualization, methodology, data curation, formal analysis, writing-original draft, writing-review and editing, and funding acquisition. JLM was responsible for conceptualization, methodology, software, data curation, formal analysis, writing-original draft, writing-review and editing. HAM was responsible for methodology, investigation, data curation, formal analysis, writing-original draft, writing-review and editing. SJ was responsible for methodology, software, data curation, formal analysis, writing-review and editing. MDR was responsible for methodology, software, data curation, formal analysis, writing-review and editing. JRC was responsible for conceptualization, methodology, writing-original draft, writing-review and editing, and funding acquisition.

Funding This work was supported by NIH grants R01 AG039684, R56 AG052576, and P30 AG072958 from the National Institute on Aging.

Data availability The data that support the findings of this study are not openly available due to reasons of sensitivity and are available from the corresponding author upon reasonable request, based on approval from the requesting researcher's local ethics committee. Data are located in controlled access data storage at the Duke University Medical Center. Depending on the nature of the request, a formal data-sharing agreement may be required.

Declarations

Conflict of interest The authors declare no conflict of interest.

References

Achard S, Bullmore E (2007) Efficiency and cost of economical brain functional networks. PLoS Comput Biol 3(2):e17. https://doi.org/10.1371/journal.pcbi.0030017

Agler R, De Boeck P (2017) On the interpretation and use of mediation: multiple perspectives on mediation analysis. Front Psychol. https://doi.org/10.3389/fpsyg.2017.01984

Alakörkkö T, Saarimäki H, Glerean E, Saramäki J, Korhonen O (2017) Effects of spatial smoothing on functional brain networks. Eur J Neurosci 46(9):2471–2480. https://doi.org/10.1111/ejn.13717

Andersson JLR, Sotiropoulos SN (2016) An integrated approach to correction for off-resonance effects and subject movement in diffusion MR imaging. Neuroimage 125:1063–1078. https://doi.org/10.1016/j.neuroimage.2015.10.019

Andrews-Hanna JR, Snyder AZ, Vincent JL, Lustig C, Head D, Raichle ME, Buckner RL (2007) Disruption of large-scale brain systems in advanced aging. Neuron 56(5):924–935

Arslan S, Ktena SI, Makropoulos A, Robinson EC, Rueckert D, Parisot S (2018) Human brain mapping: a systematic comparison of parcellation methods for the human cerebral cortex. Neuroimage 170:5–30. https://doi.org/10.1016/j.neuroimage.2017.04.014

Avants BB, Tustison NJ, Song G, Cook PA, Klein A, Gee JC (2011) A reproducible evaluation of ANTs similarity metric performance in brain image registration. Neuroimage 54(3):2033–2044. https://doi.org/10.1016/j.neuroimage.2010.09.025

Bach M (1996) The Freiburg visual acuity test—automatic measurement of visual acuity. Optom Vis Sci 73(1):49–53

Barttfeld P, Uhrig L, Sitt JD, Sigman M, Jarraya B, Dehaene S (2015) Signature of consciousness in the dynamics of resting-state brain activity. Proc Natl Acad Sci USA 112(3):887–892. https://doi.org/10.1073/pnas.1418031112

Bartzokis G (2004) Age-related myelin breakdown: a developmental model of cognitive decline and Alzheimer's disease. Neurobiol Aging 25(1):5–18

Bastiani M, Cottaar M, Fitzgibbon SP, Suri S, Alfaro-Almagro F, Sotiropoulos SN, Jbabdi S, Andersson JLR (2019) Automated quality control for within and between studies diffusion MRI data using a non-parametric framework for movement and distortion correction. Neuroimage 184:801–812. https://doi.org/10.1016/j.neuroimage.2018.09.073

Beck AT (1978) The Beck depression inventory. Psychological Corporation, New York

Bendlin BB, Fitzgerald ME, Ries ML, Xu G, Kastman EK, Thiel BW, Rowley HA, Lazar M, Alexander AL, Johnson SC (2010) White matter in aging and cognition: a cross-sectional study of microstructure in adults aged eighteen to eighty-three. Dev Neuropsychol 35(3):257–277. https://doi.org/10.1080/87565641003696775

Benjamini Y, Hochberg Y (1995) Controlling the false discovery rate: a practical and powerful approach to multiple testing. J R Stat Soc B Stat Methodol 57(1):289–300. https://doi.org/10.1111/j.2517-6161.1995.tb02031.x

Bennett IJ, Madden DJ (2014) Disconnected aging: cerebral white matter integrity and age-related differences in cognition. Neuroscience 276:187–205. https://doi.org/10.1016/j.neuroscience.2013.11.026

Bennett IJ, Motes MA, Rao NK, Rypma B (2012) White matter tract integrity predicts visual search performance in young and older adults. Neurobiol Aging 33(2):433.e421-433.e431. https://doi.org/10.1016/j.neurobiolaging.2011.02.001

Betzel RF, Byrge L, He Y, Goñi J, Zuo X-N, Sporns O (2014) Changes in structural and functional connectivity among resting-state networks across the human lifespan. Neuroimage 102(Part 2):345–357. https://doi.org/10.1016/j.neuroimage.2014.07.067

Blondel VD, Guillaume J-L, Lambiotte R, Lefebvre E (2008) Fast unfolding of communities in large networks. J Stat Mech: Theory Exp 2008(10):P10008. https://doi.org/10.1088/1742-5468/2008/10/p10008

Bolt T, Nomi JS, Rubinov M, Uddin LQ (2017) Correspondence between evoked and intrinsic functional brain network configurations. Hum Brain Mapp 38(4):1992–2007. https://doi.org/10.1002/hbm.23500

Braun U, Schafer A, Walter H, Erk S, Romanczuk-Seiferth N, Haddad L, Schweiger JI, Grimm O, Heinz A, Tost H, Meyer-Lindenberg A, Bassett DS (2015) Dynamic reconfiguration of frontal brain networks during executive cognition in humans. Proc Natl Acad Sci USA 112(37):11678–11683. https://doi.org/10.1073/pnas.1422487112

Bullmore E, Sporns O (2009) Complex brain networks: graph theoretical analysis of structural and functional systems. Nat Rev Neurosci 10(3):186–198. https://doi.org/10.1038/nrn2575

Chan MY, Park DC, Savalia NK, Petersen SE, Wig GS (2014) Decreased segregation of brain systems across the healthy adult

lifespan. Proc Natl Acad Sci USA 111(46):E4997–E5006. https://doi.org/10.1073/pnas.1415122111
Chan MY, Alhazmi FH, Park DC, Savalia NK, Wig GS (2017) Resting-state network topology differentiates task signals across the adult life span. J Neurosci 37(10):2734–2745. https://doi.org/10.1523/jneurosci.2406-16.2017
Chen G, Chen G, Xie C, Ward BD, Li W, Antuono P, Li SJ (2012) A method to determine the necessity for global signal regression in resting-state fMRI studies. Magn Reson Med 68(6):1828–1835. https://doi.org/10.1002/mrm.24201
Christensen KJ, Moye J, Armson RR, Kern TM (1992) Health screening and random recruitment for cognitive aging research. Psychol Aging 7:204–208
Ciric R, Wolf DH, Power JD, Roalf DR, Baum GL, Ruparel K, Shinohara RT, Elliott MA, Eickhoff SB, Davatzikos C, Gur RC, Gur RE, Bassett DS, Satterthwaite TD (2017) Benchmarking of participant-level confound regression strategies for the control of motion artifact in studies of functional connectivity. Neuroimage 154:174–187. https://doi.org/10.1016/j.neuroimage.2017.03.020
Ciric R, Rosen AFG, Erus G, Cieslak M, Adebimpe A, Cook PA, Bassett DS, Davatzikos C, Wolf DH, Satterthwaite TD (2018) Mitigating head motion artifact in functional connectivity MRI. Nat Protoc 13(12):2801–2826. https://doi.org/10.1038/s41596-018-0065-y
Cisler JM, Bush K, Steele JS (2014) A comparison of statistical methods for detecting context-modulated functional connectivity in fMRI. Neuroimage 84:1042–1052. https://doi.org/10.1016/j.neuroimage.2013.09.018
Civier O, Smith RE, Yeh C-H, Connelly A, Calamante F (2019) Is removal of weak connections necessary for graph-theoretical analysis of dense weighted structural connectomes from diffusion MRI? Neuroimage 194:68–81. https://doi.org/10.1016/j.neuroimage.2019.02.039
Cohen JR, D'Esposito M (2016) The segregation and integration of distinct brain networks and their relationship to cognition. J Neurosci 36(48):12083–12094. https://doi.org/10.1523/jneurosci.2965-15.2016
Cohen JR, Gallen CL, Jacobs EG, Lee TG, D'Esposito M (2014) Quantifying the reconfiguration of intrinsic networks during working memory. PLoS ONE 9(9):e106636. https://doi.org/10.1371/journal.pone.0106636
Cole MW, Bassett DS, Power JD, Braver TS, Petersen SE (2014) Intrinsic and task-evoked network architectures of the human brain. Neuron 83(1):238–251. https://doi.org/10.1016/j.neuron.2014.05.014
Cordero-Grande L, Christiaens D, Hutter J, Price AN, Hajnal JV (2019) Complex diffusion-weighted image estimation via matrix recovery under general noise models. Neuroimage 200:391–404. https://doi.org/10.1016/j.neuroimage.2019.06.039
Cox RW, Hyde JS (1997) Software tools for analysis and visualization of fMRI data. NMR Biomed 10(4–5):171–178. https://doi.org/10.1002/(SICI)1099-1492(199706/08)10:4/5%3c171::AID-NBM453%3e3.0.CO;2-L
Crossley NA, Mechelli A, Vertes PE, Winton-Brown TT, Patel AX, Ginestet CE, McGuire P, Bullmore ET (2013) Cognitive relevance of the community structure of the human brain functional coactivation network. Proc Natl Acad Sci USA 110(28):11583–11588. https://doi.org/10.1073/pnas.1220826110
Dale AM (1999) Optimal experimental design for event-related fMRI. Hum Brain Mapp 8(2–3):109–114
Damoiseaux JS, Greicius MD (2009) Greater than the sum of its parts: a review of studies combining structural connectivity and resting-state functional connectivity. Brain Struct Funct 213(6):525–533. https://doi.org/10.1007/s00429-009-0208-6
Deery HA, Di Paolo R, Moran C, Egan GF, Jamadar SD (2023) The older adult brain is less modular, more integrated, and less efficient at rest: a systematic review of large-scale resting-state functional brain networks in aging. Psychophysiology 60(1):e14159. https://doi.org/10.1111/psyp.14159
Dent K (2023) On the role of top-down and bottom-up guidance in conjunction search: Singleton interference revisited. Atten Percept Psychophys 85(6):1784–1810. https://doi.org/10.3758/s13414-023-02691-8
Du B, Cao S, Liu Y, Wei Q, Zhang J, Chen C, Wang X, Mo Y, Nie J, Qiu B, Hu P, Wang K (2021) Abnormal degree centrality in white matter hyperintensities: a resting-state functional magnetic resonance imaging study. Front Psychiatry 12:684553. https://doi.org/10.3389/fpsyt.2021.684553
Dutilh G, Annis J, Brown SD, Cassey P, Evans NJ, Grasman R, Hawkins GE, Heathcote A, Holmes WR, Krypotos AM, Kupitz CN, Leite FP, Lerche V, Lin YS, Logan GD, Palmeri TJ, Starns JJ, Trueblood JS, van Maanen L, van Ravenzwaaij D, Vandekerckhove J, Visser I, Voss A, White CN, Wiecki TV, Rieskamp J, Donkin C (2019) The quality of response time data inference: a blinded, collaborative assessment of the validity of cognitive models. Psychon Bull Rev 26:1051–1069. https://doi.org/10.3758/s13423-017-1417-2
Dvorine I (1963) Dvorine pseudo-isochromatic plates, 2nd edn. Harcourt, New York
Elton A, Gao W (2015) Task-related modulation of functional connectivity variability and its behavioral correlations. Hum Brain Mapp 36(8):3260–3272. https://doi.org/10.1002/hbm.22847
Esteban O, Markiewicz CJ, Blair RW, Moodie CA, Isik AI, Erramuzpe A, Kent JD, Goncalves M, DuPre E, Snyder M, Oya H, Ghosh SS, Wright J, Durnez J, Poldrack RA, Gorgolewski KJ (2019) fMRIPrep: a robust preprocessing pipeline for functional MRI. Nat Methods 16(1):111–116. https://doi.org/10.1038/s41592-018-0235-4
Fan L, Li H, Zhuo J, Zhang Y, Wang J, Chen L, Yang Z, Chu C, Xie S, Laird AR, Fox PT, Eickhoff SB, Yu C, Jiang T (2016) The Human Brainnetome Atlas: a new brain atlas based on connectional architecture. Cereb Cortex 26(8):3508–3526. https://doi.org/10.1093/cercor/bhw157
Fjell AM, Sneve MH, Grydeland H, Storsve AB, Walhovd KB (2016) The disconnected brain and executive function decline in aging. Cereb Cortex 27(3):2303–2317. https://doi.org/10.1093/cercor/bhw082
Fjell AM, Sneve MH, Grydeland H, Storsve AB, Amlien IK, Yendiki A, Walhovd KB (2017) Relationship between structural and functional connectivity change across the adult lifespan: a longitudinal investigation. Hum Brain Mapp 38(1):561–573. https://doi.org/10.1002/hbm.23403
Folstein MF, Folstein SE, McHugh PR (1975) "Mini-mental state". A practical method for grading the cognitive state of patients for the clinician. J Psychiatr Res 12(3):189–198
Fukushima M, Betzel RF, He Y, van den Heuvel MP, Zuo X-N, Sporns O (2018) Structure–function relationships during segregated and integrated network states of human brain functional connectivity. Brain Struct Funct 223(3):1091–1106. https://doi.org/10.1007/s00429-017-1539-3
Gallen CL, Turner GR, Adnan A, D'Esposito M (2016) Reconfiguration of brain network architecture to support executive control in aging. Neurobiol Aging 44:42–52. https://doi.org/10.1016/j.neurobiolaging.2016.04.003
Geerligs L, Saliasi E, Renken RJ, Maurits NM, Lorist MM (2014) Flexible connectivity in the aging brain revealed by task modulations. Hum Brain Mapp 35(8):3788–3804. https://doi.org/10.1002/hbm.22437
Goh JO (2011) Functional dedifferentiation and altered connectivity in older adults: neural accounts of cognitive aging. Aging Dis 2(1):30–48

Gong G, He Y, Concha L, Lebel C, Gross DW, Evans AC, Beaulieu C (2009) Mapping anatomical connectivity patterns of human cerebral cortex using in vivo diffusion tensor imaging tractography. Cereb Cortex 19(3):524–536. https://doi.org/10.1093/cercor/bhn102

Gordon EM, Laumann TO, Adeyemo B, Huckins JF, Kelley WM, Petersen SE (2014) Generation and evaluation of a cortical area parcellation from resting-state correlations. Cereb Cortex 26(1):288–303. https://doi.org/10.1093/cercor/bhu239

Grady C, Sarraf S, Saverino C, Campbell K (2016) Age differences in the functional interactions among the default, frontoparietal control, and dorsal attention networks. Neurobiol Aging 41:159–172. https://doi.org/10.1016/j.neurobiolaging.2016.02.020

Greve DN, Fischl B (2009) Accurate and robust brain image alignment using boundary-based registration. Neuroimage 48(1):63–72. https://doi.org/10.1016/j.neuroimage.2009.06.060

Guevara M, Guevara P, Román C, Mangin J-F (2020) Superficial white matter: a review on the dMRI analysis methods and applications. Neuroimage 212:116673. https://doi.org/10.1016/j.neuroimage.2020.116673

Hagmann P, Kurant M, Gigandet X, Thiran P, Wedeen VJ, Meuli R, Thiran J-P (2007) Mapping human whole-brain structural networks with diffusion MRI. PLoS ONE 2(7):e597. https://doi.org/10.1371/journal.pone.0000597

Hagmann P, Cammoun L, Gigandet X, Meuli R, Honey CJ, Wedeen VJ, Sporns O (2008) Mapping the structural core of human cerebral cortex. PLoS Biol 6(7):e159. https://doi.org/10.1016/j.neuroimage.2011.09.015

Hayes AF (2013) Introduction to mediation, moderation, and conditional process analysis. Guilford, New York

Hayes AF, Rockwood NJ (2017) Regression-based statistical mediation and moderation analysis in clinical research: observations, recommendations, and implementation. Behav Res Ther 98(Supplement C):39–57. https://doi.org/10.1016/j.brat.2016.11.001

He J, Carmichael O, Fletcher E, Singh B, Iosif AM, Martinez O, Reed B, Yonelinas A, Decarli C (2012) Influence of functional connectivity and structural MRI measures on episodic memory. Neurobiol Aging 33(11):2612–2620. https://doi.org/10.1016/j.neurobiolaging.2011.12.029

Hearne LJ, Cocchi L, Zalesky A, Mattingley JB (2017) Reconfiguration of brain network architectures between resting-state and complexity-dependent cognitive reasoning. J Neurosci 37(35):8399–8411. https://doi.org/10.1523/jneurosci.0485-17.2017

Hofer SM, Sliwinski MJ (2001) Understanding ageing. An evaluation of research designs for assessing the interdependence of ageing-related changes. Gerontology 47(6):341–352. https://doi.org/10.1159/000052825

Hommel B, Li KZ, Li SC (2004) Visual search across the life span. Dev Psychol 40(4):545–558. https://doi.org/10.1037/0012-1649.40.4.545

Honey CJ, Kötter R, Breakspear M, Sporns O (2007) Network structure of cerebral cortex shapes functional connectivity on multiple time scales. Proc Natl Acad Sci USA 104(24):10240–10245. https://doi.org/10.1073/pnas.0701519104

Honey CJ, Sporns O, Cammoun L, Gigandet X, Thiran JP, Meuli R, Hagmann P (2009) Predicting human resting-state functional connectivity from structural connectivity. Proc Natl Acad Sci USA 106(6):2035–2040. https://doi.org/10.1073/pnas.0811168106

Hughes C, Faskowitz J, Cassidy BS, Sporns O, Krendl AC (2020) Aging relates to a disproportionately weaker functional architecture of brain networks during rest and task states. Neuroimage 209:116521. https://doi.org/10.1016/j.neuroimage.2020.116521

Ji JL, Spronk M, Kulkarni K, Repovs G, Anticevic A, Cole MW (2019) Mapping the human brain's cortical-subcortical functional network organization. Neuroimage 185:35–57. https://doi.org/10.1016/j.neuroimage.2018.10.006

Kramer AF, Madden DJ (2008) Attention. In: Craik FIM, Salthouse TA (eds) The handbook of aging and cognition, 3rd edn. Psychology Press, New York, pp 189–249

Krienen FM, Yeo BTT, Buckner RL (2014) Reconfigurable task-dependent functional coupling modes cluster around a core functional architecture. Philos Trans R Soc Lond B Biol Sci 369(1653):20130526. https://doi.org/10.1098/rstb.2013.0526

Lancichinetti A, Fortunato S (2012) Consensus clustering in complex networks. Sci Rep 2:336. https://doi.org/10.1038/srep00336

Li J, Kong R, Liégeois R, Orban C, Tan Y, Sun N, Holmes AJ, Sabuncu MR, Ge T, Yeo BTT (2019) Global signal regression strengthens association between resting-state functional connectivity and behavior. Neuroimage 196:126–141. https://doi.org/10.1016/j.neuroimage.2019.04.016

Lindenberger U, von Oertzen T, Ghisletta P, Hertzog C (2011) Cross-sectional age variance extraction: What's change got to do with it? Psychol Aging 26(1):34–47. https://doi.org/10.1037/a0020525

Lu T, Wang Z, Zhu Y, Wang M, Lu C-Q, Ju S (2024) Long-range connections damage in white matter hyperintensities affects information processing speed. Brain Commun. https://doi.org/10.1093/braincomms/fcae042

Madden DJ (2001) Speed and timing of behavioral processes. In: Birren JE, Schaie KW (eds) Handbook of the psychology of aging, 5th edn. Academic Press, San Diego, pp 288–312

Madden DJ (2007) Aging and visual attention. Curr Dir Psychol Sci 16(2):70–74. https://doi.org/10.1111/j.1467-8721.2007.00478.x

Madden DJ, Monge ZA (2019) Visual attention with cognitive aging. In: Oxford research encyclopedia of psychology. Oxford University Press, Oxford. https://doi.org/10.1093/acrefore/9780190236557.013.369

Madden DJ, Costello MC, Dennis NA, Davis SW, Shepler AM, Spaniol J, Bucur B, Cabeza R (2010) Adult age differences in functional connectivity during executive control. Neuroimage 52(2):643–657. https://doi.org/10.1016/j.neuroimage.2010.04.249

Madden DJ, Bennett IJ, Burzynska A, Potter GG, Chen NK, Song AW (2012) Diffusion tensor imaging of cerebral white matter integrity in cognitive aging. Biochim Biophys Acta 1822(3):386–400. https://doi.org/10.1016/j.bbadis.2011.08.003

Madden DJ, Parks EL, Tallman CW, Boylan MA, Hoagey DA, Cocjin SB, Johnson MA, Chou Y-h, Potter GG, Chen N-k, Packard LE, Siciliano RE, Monge ZA, Diaz MT (2017a) Frontoparietal activation during visual conjunction search: effects of bottom-up guidance and adult age. Hum Brain Mapp 38(4):2128–2149. https://doi.org/10.1002/hbm.23509

Madden DJ, Parks EL, Tallman CW, Boylan MA, Hoagey DA, Cocjin SB, Packard LE, Johnson MA, Chou Y-h, Potter GG, Chen N-k, Siciliano RE, Monge ZA, Honig JA, Diaz MT (2017b) Sources of disconnection in neurocognitive aging: cerebral white-matter integrity, resting-state functional connectivity, and white-matter hyperintensity volume. Neurobiol Aging 54:199–213. https://doi.org/10.1016/j.neurobiolaging.2017.01.027

Madden DJ, Jain S, Monge ZA, Cook AD, Lee A, Huang H, Howard CM, Cohen JR (2020a) Influence of structural and functional brain connectivity on age-related differences in fluid cognition. Neurobiol Aging 96:205–222. https://doi.org/10.1016/j.neurobiolaging.2020.09.010

Madden DJ, Siciliano RE, Tallman CW, Monge ZA, Voss A, Cohen JR (2020b) Response-level processing during visual feature search: Effects of frontoparietal activation and adult age. Atten Percept Psychophys 82(1):330–349. https://doi.org/10.3758/s13414-019-01823-3

Malagurski B, Liem F, Oschwald J, Mérillat S, Jäncke L (2020) Functional dedifferentiation of associative resting state networks in older adults—a longitudinal study. Neuroimage 214:116680. https://doi.org/10.1016/j.neuroimage.2020.116680

Maxwell SE, Cole DA (2007) Bias in cross-sectional analyses of longitudinal mediation. Psychol Methods 12(1):23–44. https://doi.org/10.1037/1082-989X.12.1.23

Meilă M (2007) Comparing clusterings—an information based distance. J Multivar Anal 98(5):873–895. https://doi.org/10.1016/j.jmva.2006.11.013

Merenstein JL, Mullin HA, Madden DJ (2023) Age-related differences in frontoparietal activation for target and distractor singletons during visual search. Atten Percept Psychophys 85(3):749–768. https://doi.org/10.3758/s13414-022-02640-x

Mišić B, Sporns O (2016) From regions to connections and networks: new bridges between brain and behavior. Curr Opin Neurobiol 40:1–7. https://doi.org/10.1016/j.conb.2016.05.003

Mišić B, Betzel RF, de Reus MA, van den Heuvel MP, Berman MG, McIntosh AR, Sporns O (2016) Network-level structure–function relationships in human neocortex. Cereb Cortex 26(7):3285–3296. https://doi.org/10.1093/cercor/bhw089

Monge ZA, Geib BR, Siciliano RE, Packard LE, Tallman CW, Madden DJ (2017) Functional modular architecture underlying attentional control in aging. Neuroimage 155:257–270. https://doi.org/10.1016/j.neuroimage.2017.05.002

Mumford JA, Turner BO, Ashby FG, Poldrack RA (2012) Deconvolving BOLD activation in event-related designs for multivoxel pattern classification analyses. Neuroimage 59(3):2636–2643. https://doi.org/10.1016/j.neuroimage.2011.08.076

Murphy K, Fox MD (2017) Towards a consensus regarding global signal regression for resting state functional connectivity MRI. Neuroimage 154:169–173. https://doi.org/10.1016/j.neuroimage.2016.11.052

Newman ME, Girvan M (2004) Finding and evaluating community structure in networks. Phys Rev E Stat Nonlin Soft Matter Phys 69(2 Pt 2):026113. https://doi.org/10.1103/PhysRevE.69.026113

Ng KK, Lo JC, Lim JKW, Chee MWL, Zhou J (2016) Reduced functional segregation between the default mode network and the executive control network in healthy older adults: a longitudinal study. Neuroimage 133:321–330. https://doi.org/10.1016/j.neuroimage.2016.03.029

Oldham S, Arnatkevičiūtė A, Smith RE, Tiego J, Bellgrove MA, Fornito A (2020) The efficacy of different preprocessing steps in reducing motion-related confounds in diffusion MRI connectomics. Neuroimage 222:117252. https://doi.org/10.1016/j.neuroimage.2020.117252

Parkes L, Fulcher B, Yücel M, Fornito A (2018) An evaluation of the efficacy, reliability, and sensitivity of motion correction strategies for resting-state functional MRI. Neuroimage 171:415–436. https://doi.org/10.1016/j.neuroimage.2017.12.073

Pedersen R, Geerligs L, Andersson M, Gorbach T, Avelar-Pereira B, Wåhlin A, Rieckmann A, Nyberg L, Salami A (2021) When functional blurring becomes deleterious: reduced system segregation is associated with less white matter integrity and cognitive decline in aging. Neuroimage 242:118449. https://doi.org/10.1016/j.neuroimage.2021.118449

Power JD, Cohen AL, Nelson SM, Wig GS, Barnes KA, Church JA, Vogel AC, Laumann TO, Miezin FM, Schlaggar BL, Petersen SE (2011) Functional network organization of the human brain. Neuron 72(4):665–678. https://doi.org/10.1016/j.neuron.2011.09.006

Power JD, Barnes KA, Snyder AZ, Schlaggar BL, Petersen SE (2012) Spurious but systematic correlations in functional connectivity MRI networks arise from subject motion. Neuroimage 59(3):2142–2154. https://doi.org/10.1016/j.neuroimage.2011.10.018

Power JD, Mitra A, Laumann TO, Snyder AZ, Schlaggar BL, Petersen SE (2014) Methods to detect, characterize, and remove motion artifact in resting state fMRI. Neuroimage 84:320–341. https://doi.org/10.1016/j.neuroimage.2013.08.048

Puxeddu MG, Faskowitz J, Betzel RF, Petti M, Astolfi L, Sporns O (2020) The modular organization of brain cortical connectivity across the human lifespan. Neuroimage 218:116974. https://doi.org/10.1016/j.neuroimage.2020.116974

Rabbitt P (2017) Speed of visual search in old age: 1950 to 2016. J Gerontol B Psychol Sci Soc Sci 72(1):51–60. https://doi.org/10.1093/geronb/gbw097

Rabbitt P, Scott M, Lunn M, Thacker N, Lowe C, Pendleton N, Horan M, Jackson A (2007) White matter lesions account for all age-related declines in speed but not in intelligence. Neuropsychology 21(3):363–370. https://doi.org/10.1037/0894-4105.21.3.363

Ratcliff R (2008) Modeling aging effects on two-choice tasks: response signal and response time data. Psychol Aging 23(4):900–916. https://doi.org/10.1037/a0013930

Ratcliff R, McKoon G (2008) The diffusion decision model: theory and data for two-choice decision tasks. Neural Comput 20(4):873–922. https://doi.org/10.1162/neco.2008.12-06-420

Ratcliff R, Smith PL, Brown SD, McKoon G (2016) Diffusion decision model: current issues and history. Trends Cogn Sci 20(4):260–281. https://doi.org/10.1016/j.tics.2016.01.007

Reichardt J, Bornholdt S (2006) Statistical mechanics of community detection. Phys Rev E Stat Nonlin Soft Matter Phys. https://doi.org/10.1103/PhysRevE.74.016110

Rissman J, Gazzaley A, D'Esposito M (2004) Measuring functional connectivity during distinct stages of a cognitive task. Neuroimage 23(2):752–763

Roski C, Caspers S, Langner R, Laird A, Fox P, Zilles K, Amunts K, Eickhoff S (2013) Adult age-dependent differences in resting-state connectivity within and between visual-attention and sensorimotor networks. Front Aging Neurosci. https://doi.org/10.3389/fnagi.2013.00067

Rubinov M, Sporns O (2010) Complex network measures of brain connectivity: uses and interpretations. Neuroimage 52(3):1059–1069. https://doi.org/10.1016/j.neuroimage.2009.10.003

Rubinov M, Sporns O (2011) Weight-conserving characterization of complex functional brain networks. Neuroimage 56(4):2068–2079. https://doi.org/10.1016/j.neuroimage.2011.03.069

Salami A, Eriksson J, Nilsson LG, Nyberg L (2012) Age-related white matter microstructural differences partly mediate age-related decline in processing speed but not cognition. Biochim Biophys Acta 1822(3):408–415. https://doi.org/10.1016/j.bbadis.2011.09.001

Salat DH (2011) The declining infrastructure of the aging brain. Brain Connect 1(4):279–293. https://doi.org/10.1089/brain.2011.0056

Salthouse TA (1985) Speed of behavior and its implications for cognition. In: Birren JE, Schaie KW (eds) Handbook of the psychology of aging, 2nd edn. Van Nostrand Reinhold, New York, pp 400–426

Salthouse TA (1996) The processing-speed theory of adult age differences in cognition. Psychol Rev 103(3):403–428. https://doi.org/10.1037/0033-295x.103.3.403

Salthouse TA (2011a) All data collection and analysis methods have limitations: Reply to Rabbitt (2011) and Raz and Lindenberger (2011). Psychol Bull 137(5):796–799. https://doi.org/10.1037/a0024843

Salthouse TA (2011b) Neuroanatomical substrates of age-related cognitive decline. Psychol Bull 137(5):753–784. https://doi.org/10.1037/a0023262

Salthouse TA, Madden DJ (2007) Information processing speed and aging. In: Deluca J, Kalmar J (eds) Information processing speed in clinical populations. Psychology Press, New York, pp 221–241

Salthouse TA, Nesselroade JR (2002) An examination of the Hofer and Sliwinski evaluation. Gerontology 48(1):18–21. https://doi.org/10.1159/000048919

Sams EC (2021) Oligodendrocytes in the aging brain. Neuronal Signal. https://doi.org/10.1042/ns20210008
Satterthwaite TD, Elliott MA, Gerraty RT, Ruparel K, Loughead J, Calkins ME, Eickhoff SB, Hakonarson H, Gur RC, Gur RE, Wolf DH (2013) An improved framework for confound regression and filtering for control of motion artifact in the preprocessing of resting-state functional connectivity data. Neuroimage 64:240–256. https://doi.org/10.1016/j.neuroimage.2012.08.052
Schulz M, Mayer C, Schlemm E, Frey BM, Malherbe C, Petersen M, Gallinat J, Kühn S, Fiehler J, Hanning U, Twerenbold R, Gerloff C, Cheng B, Thomalla G (2022) Association of age and structural brain changes with functional connectivity and executive function in a middle-aged to older population-based cohort. Front Aging Neurosci. https://doi.org/10.3389/fnagi.2022.782738
Servant M, Evans NJ (2020) A diffusion model analysis of the effects of aging in the Flanker Task. Psychol Aging 35(6):831–849. https://doi.org/10.1037/pag0000546
Shine JM, Bissett PG, Bell PT, Koyejo O, Balsters JH, Gorgolewski KJ, Moodie CA, Poldrack RA (2016) The dynamics of functional brain networks: integrated network states during cognitive task performance. Neuron 92(2):544–554. https://doi.org/10.1016/j.neuron.2016.09.018
Smith SM, Jenkinson M, Woolrich MW, Beckmann CF, Behrens TE, Johansen-Berg H, Bannister PR, De Luca M, Drobnjak I, Flitney DE, Niazy RK, Saunders J, Vickers J, Zhang Y, De Stefano N, Brady JM, Matthews PM (2004) Advances in functional and structural MR image analysis and implementation as FSL. Neuroimage 23(Suppl 1):S208-219. https://doi.org/10.1016/j.neuroimage.2004.07.051
Smith RE, Tournier J-D, Calamante F, Connelly A (2012) Anatomically-constrained tractography: improved diffusion MRI streamlines tractography through effective use of anatomical information. Neuroimage 62(3):1924–1938. https://doi.org/10.1016/j.neuroimage.2012.06.005
Smith RE, Tournier J-D, Calamante F, Connelly A (2013) SIFT: spherical-deconvolution informed filtering of tractograms. Neuroimage 67:298–312. https://doi.org/10.1016/j.neuroimage.2012.11.049
Smith RE, Tournier JD, Calamante F, Connelly A (2015) The effects of SIFT on the reproducibility and biological accuracy of the structural connectome. Neuroimage 104:253–265. https://doi.org/10.1016/j.neuroimage.2014.10.004
Spadone S, Della Penna S, Sestieri C, Betti V, Tosoni A, Perrucci MG, Romani GL, Corbetta M (2015) Dynamic reorganization of human resting-state networks during visuospatial attention. Proc Natl Acad Sci USA 112(26):8112–8117. https://doi.org/10.1073/pnas.1415439112
Sporns O (2011) The human connectome: a complex network. Ann N Y Acad Sci 1224(1):109–125. https://doi.org/10.1111/j.1749-6632.2010.05888.x
Sporns O, Betzel RF (2016) Modular brain networks. Annu Rev Psychol 67(1):613–640. https://doi.org/10.1146/annurev-psych-122414-033634
Spreng RN, Stevens WD, Viviano JD, Schacter DL (2016) Attenuated anticorrelation between the default and dorsal attention networks with aging: evidence from task and rest. Neurobiol Aging 45:149–160. https://doi.org/10.1016/j.neurobiolaging.2016.05.020
Steiger JH (1980) Tests for comparing elements of a correlation matrix. Psychol Bull 87(2):245–251. https://doi.org/10.1037/0033-2909.87.2.245
Theeuwes J (2010) Top-down and bottom-up control of visual selection. Acta Psychol (Amst) 135(2):77–99. https://doi.org/10.1016/j.actpsy.2010.02.006
Tournier J-D, Smith R, Raffelt D, Tabbara R, Dhollander T, Pietsch M, Christiaens D, Jeurissen B, Yeh C-H, Connelly A (2019) MRtrix3: a fast, flexible and open software framework for medical image processing and visualisation. Neuroimage 202:116137. https://doi.org/10.1016/j.neuroimage.2019.116137
Treiber JM, White NS, Steed TC, Bartsch H, Holland D, Farid N, McDonald CR, Carter BS, Dale AM, Chen CC (2016) Characterization and correction of geometric distortions in 814 diffusion weighted images. PLoS ONE 11(3):e0152472. https://doi.org/10.1371/journal.pone.0152472
Tuladhar AM, van Dijk E, Zwiers MP, van Norden AGW, de Laat KF, Shumskaya E, Norris DG, de Leeuw F-E (2016) Structural network connectivity and cognition in cerebral small vessel disease. Hum Brain Mapp 37(1):300–310. https://doi.org/10.1002/hbm.23032
Van Dijk KR, Sabuncu MR, Buckner RL (2012) The influence of head motion on intrinsic functional connectivity MRI. Neuroimage 59(1):431–438. https://doi.org/10.1016/j.neuroimage.2011.07.044
van Ravenzwaaij D, Oberauer K (2009) How to use the diffusion model: Parameter recovery of three methods: EZ, fast-dm, and DMAT. J Math Psychol 53(6):463–473. https://doi.org/10.1016/j.jmp.2009.09.004
van Wijk BCM, Stam CJ, Daffertshofer A (2010) Comparing brain networks of different size and connectivity density using graph theory. PLoS ONE 5(10):e13701. https://doi.org/10.1371/journal.pone.0013701
Veraart J, Novikov DS, Christiaens D, Ades-Aron B, Sijbers J, Fieremans E (2016) Denoising of diffusion MRI using random matrix theory. Neuroimage 142:394–406. https://doi.org/10.1016/j.neuroimage.2016.08.016
Voss A, Nagler M, Lerche V (2013) Diffusion models in experimental psychology: a practical introduction. Exp Psychol 60(6):385–402. https://doi.org/10.1027/1618-3169/a000218
Wagenmakers E-J, Van Der Maas HLJ, Grasman RPPP (2007) An EZ-diffusion model for response time and accuracy. Psychon Bull Rev 14(1):3–22. https://doi.org/10.3758/BF03194023
Wechsler D (1997) Wechsler adult intelligence scale-III. Psychological Corporation, New York
Wen X, Zhang D, Liang B, Zhang R, Wang Z, Wang J, Liu M, Huang R (2015) Reconfiguration of the brain functional network associated with visual task demands. PLoS ONE 10(7):e0132518. https://doi.org/10.1371/journal.pone.0132518
Wig GS (2017) Segregated systems of human brain networks. Trends Cogn Sci 21(12):981–996. https://doi.org/10.1016/j.tics.2017.09.006
Wolfe JM, Horowitz TS (2004) What attributes guide the deployment of visual attention and how do they do it? Nat Rev Neurosci 5(6):495–501. https://doi.org/10.1038/nrn1411
Woolrich MW, Ripley BD, Brady M, Smith SM (2001) Temporal autocorrelation in univariate linear modeling of FMRI data. Neuroimage 14(6):1370–1386. https://doi.org/10.1006/nimg.2001.0931
Wöstmann M, Störmer VS, Obleser J, Addleman DA, Andersen SK, Gaspelin N, Geng JJ, Luck SJ, Noonan MP, Slagter HA, Theeuwes J (2022) Ten simple rules to study distractor suppression. Prog Neurobiol 213:102269. https://doi.org/10.1016/j.pneurobio.2022.102269
Wu K, Taki Y, Sato K, Kinomura S, Goto R, Okada K, Kawashima R, He Y, Evans AC, Fukuda H (2012) Age-related changes in topological organization of structural brain networks in healthy individuals. Hum Brain Mapp 33(3):552–568. https://doi.org/10.1002/hbm.21232
Wu M, Kumar A, Yang S (2016) Development and aging of superficial white matter myelin from young adulthood to old age: mapping by vertex-based surface statistics (VBSS). Hum Brain Mapp 37(5):1759–1769. https://doi.org/10.1002/hbm.23134
Yantis S (1996) Attentional capture in vision. In: Kramer AF, Coles GH, Logan GD (eds) Coverging operations in the study of visual

selective attention. American Psychological Association, Washington, DC, pp 45–76

Yeh C-H, Smith RE, Liang X, Calamante F, Connelly A (2016) Correction for diffusion MRI fibre tracking biases: the consequences for structural connectomic metrics. Neuroimage 142:150–162. https://doi.org/10.1016/j.neuroimage.2016.05.047

Yeo BT, Krienen FM, Sepulcre J, Sabuncu MR, Lashkari D, Hollinshead M, Roffman JL, Smoller JW, Zollei L, Polimeni JR, Fischl B, Liu H, Buckner RL (2011) The organization of the human cerebral cortex estimated by intrinsic functional connectivity. J Neurophysiol 106(3):1125–1165. https://doi.org/10.1152/jn.00338.2011

Zalesky A, Fornito A, Harding IH, Cocchi L, Yucel M, Pantelis C, Bullmore ET (2010) Whole-brain anatomical networks: Does the choice of nodes matter? Neuroimage 50(3):970–983. https://doi.org/10.1016/j.neuroimage.2009.12.027

Zamani Esfahlani F, Faskowitz J, Slack J, Mišić B, Betzel RF (2022) Local structure–function relationships in human brain networks across the lifespan. Nat Commun 13(1):2053. https://doi.org/10.1038/s41467-022-29770-y

Zhang H, Gertel VH, Cosgrove AL, Diaz MT (2021) Age-related differences in resting-state and task-based network characteristics and cognition: a lifespan sample. Neurobiol Aging 101:262–272. https://doi.org/10.1016/j.neurobiolaging.2020.10.025

Zhang F, Daducci A, He Y, Schiavi S, Seguin C, Smith RE, Yeh C-H, Zhao T, O'Donnell LJ (2022) Quantitative mapping of the brain's structural connectivity using diffusion MRI tractography: a review. Neuroimage 249:118870. https://doi.org/10.1016/j.neuroimage.2021.118870

Zhao T, Cao M, Niu H, Zuo X-N, Evans A, He Y, Dong Q, Shu N (2015) Age-related changes in the topological organization of the white matter structural connectome across the human lifespan. Hum Brain Mapp 36(10):3777–3792. https://doi.org/10.1002/hbm.22877

Zimmermann J, Ritter P, Shen K, Rothmeier S, Schirner M, McIntosh AR (2016) Structural architecture supports functional organization in the human aging brain at a regionwise and network level. Hum Brain Mapp 37(7):2645–2661. https://doi.org/10.1002/hbm.23200

Zuo X-N, He Y, Betzel RF, Colcombe S, Sporns O, Milham MP (2017) Human connectomics across the life span. Trends Cogn Sci 21(1):32–45. https://doi.org/10.1016/j.tics.2016.10.005